



HAL
open science

Hydrochemical constraints between the karst Tabular Middle Atlas Causses and the Sais basin (Morocco): implications of groundwater circulation

Helene Miche, Ginette Saracco, Adriano Mayer, Khaoula Qarqori, Mohamed Rouai, Abdelilah Dekayir, Konstantinos Chalikakis, Christophe Emblanch

► To cite this version:

Helene Miche, Ginette Saracco, Adriano Mayer, Khaoula Qarqori, Mohamed Rouai, et al.. Hydrochemical constraints between the karst Tabular Middle Atlas Causses and the Sais basin (Morocco): implications of groundwater circulation. *Hydrogeology Journal*, 2018, 26 (1), pp.71-87. 10.1007/s10040-017-1675-0 . hal-01970695

HAL Id: hal-01970695

<https://hal.science/hal-01970695>

Submitted on 16 Jan 2019

HAL is a multi-disciplinary open access archive for the deposit and dissemination of scientific research documents, whether they are published or not. The documents may come from teaching and research institutions in France or abroad, or from public or private research centers.

L'archive ouverte pluridisciplinaire **HAL**, est destinée au dépôt et à la diffusion de documents scientifiques de niveau recherche, publiés ou non, émanant des établissements d'enseignement et de recherche français ou étrangers, des laboratoires publics ou privés.



Distributed under a Creative Commons Attribution - NonCommercial 4.0 International License

Hydrochemical constraints between the karst Tabular Middle Atlas Causses and the Saïs basin (Morocco): implications of groundwater circulation

Hélène Miche¹ · Ginette Saracco¹ · Adriano Mayer^{1,2} · Khaoula Qarqori³ · Mohamed Rouai³ · Abdelilah Dekayir³ · Konstantinos Chalikakis² · Christophe Emblanch²

Abstract The karst Tabular Middle Atlas Causses reservoir is the main drinking-water supply of Fez-Meknes region (Saïs Basin) in Morocco. Recent analyses showed a decline in associated groundwater chemical quality and increased turbidity. To understand this hydrosystem, four surveys were undertaken during fall and spring, 2009–2011. Hydrogeochemical studies coupled with isotopic analyses ($\delta^{18}\text{O}$, δD and ^{222}Rn) showed that the aquifers between the causses (mountains) and the Saïs Basin are of Liassic origin and at the southern extremities are of Triassic origin. Five recharge zones of different altitudes have been defined, including two main mixing zones in the south. Deuterium excess results suggest local recharge, while a plot of $\delta^{18}\text{O}$ versus δD characterizes a confined aquifer in the eastern sector. ^{222}Rn results reveal areas of rapid exchanges with an upwelling time of less than 2 weeks. A schematic conceptual model is presented to explain the groundwater circulation system and the behavior of this karst system.

Keywords Morocco · Hydrochemistry · Isotopic analyses · Conceptual models · Groundwater flow

Introduction

The study area is located at the junction of the Tabular Middle Atlas (TMA) mountains and the plain of Saïs. The plain of Saïs is bordered in the south by the Tabular Middle Atlas (TMA), in the north by the pre-Rif ridges, in the west by the Rharb plain, and in the east by the Fez-Taza corridor (Fig. 1). The plain of Saïs is very important for agriculture in Morocco and has a population of 1.6 million inhabitants, with two important cities, Fez to the east and Meknes to the west.

Population growth in the region, the intensive farming and industrial development, and the recurrence of drought

✉ Hélène Miche
miche@cerege.fr

Ginette Saracco
saracco@cerege.fr

Adriano Mayer
adriano.mayer@univ-avignon.fr

Khaoula Qarqori
khqarqori@gmail.com

Mohamed Rouai
mohamed.rouai@laposte.net

Abdelilah Dekayir
dekayir@yahoo.fr

Konstantinos Chalikakis
konstantinos.chalikakis@univ-avignon.fr

Christophe Emblanch
christophe.emblanch@univ-avignon.fr

¹ CNRS-UMR 7330, CEREGE, Aix-Marseille Université, IRD, Europôle de l'Arbois, BP 80, 13545 Aix en Provence, Cedex 4, France

² Université d'Avignon et des Pays de Vaucluse, INRA, EMMAH, UMR 1114, LHA, 84000 Avignon, France

³ Faculté des Sciences, Département des Sciences de la Terre, Université Moulay Ismail, BP 11201, 50000 Meknès, Morocco

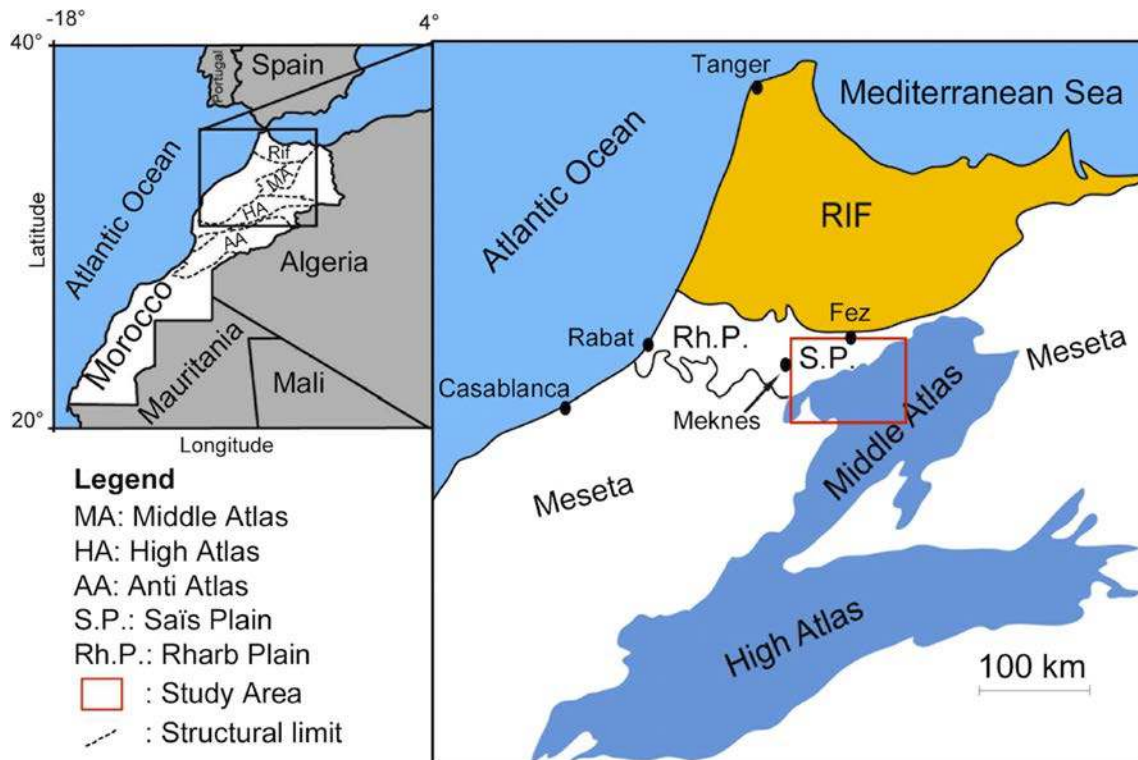


Fig. 1 Geographical localisation of the study area (red rectangle) between the Saïs Basin and Middle Atlas Causse (Morocco; Qarqori 2015)

(Amraoui et al. 2004; Bzioui 2004; Amraoui et al. 2005; Luterbacher et al. 2006; Esper et al. 2007; Etebaai et al. 2012) impact and affect groundwater management and the capacity to ensure a sufficient supply, in terms of both quantity and quality, for surrounding towns and villages over time. In this context, knowledge of water circulation pathways and of the seasonal variations of groundwater resources becomes a key issue for resource preservation and the mitigation of possible desertification or soil degradation.

The TMA is mainly constituted by Liassic limestone-dolomite formations (Fig. 2), which have an important hydrological potential (Kabbaj and Combe 1977; Bentayeb and Leclerc 1977). These Liassic carbonates dip northward at the junction of TMA with the Saïs basin, beneath a thick Miocene marls deposit, and constitute a confined aquifer (Fig. 3). At the TMA/Saïs basin junction, several outlets as karst springs drain a part of the groundwater flow. “Ribaa-Bittit” complex is the most important one.

In the Saïs basin, the Liassic and Miocene formations overlay the Triassic clays, basalts and evaporites, and are overlain by Pliocene-Quaternary limestone and travertine (Chamayou et al. 1975; Figs. 2 and 3). These carbonates are affected by several fractures causing a dislocation of different Liassic blocs and sometimes Pliocene-Quaternary limestone-travertine (Bentayeb and Leclerc 1977; Martin 1981). The groundwater flows in this region are conditioned by two major fracture networks, mainly NE–SW and NW–SE directions (Bentayeb and Leclerc 1977; Essahlaoui et al. 2001;

Amraoui 2005), and probably with a NW–SE preferential flow direction (Qarqori et al. 2012). A karstic complex water circulation is especially developed locally at the border of the two hydrogeological units (Qarqori 2015).

The deep and shallow aquifers of Saïs basin, supplied by rainfall and TMA water, and the springs located on the TMA/Saïs basin contact boundary represent the most important water supply of the region for drinking and agricultural uses (Bahaj et al. 2004; Belkhiri 2007; Benaabidate and Fryar 2010). However, the modalities of water transfer between the Middle Atlas Causses and Saïs basin and the interactions of water with the different geological facies are not well known.

The purpose of the study was to understand the groundwater flows and their renewal in this densely populated region suffering water resources overexploitation, and this paper explains the methods and outcomes. Constraints on the groundwater flow paths have been obtained by coupling hydrochemical and isotopic characterization of the water samples from springs and wells.

Geochemical and isotopic results (major and minor elements, $\delta^{18}\text{O}$, δD and ^{222}Rn) are presented for the main ten springs and three wells (from different geological origins) studied between 2009 and 2011 around the Ribaa-Bittit springs complex and along the transition zone (study area of $70 \times 40 \text{ km}^2$) between the Saïs basin and the TMA reservoir (Figs. 1 and 2). The ten springs studied included Bittit; Ribaa; Aguemguam; Sbaa; El Mir; Boucharmou; Bou Youssef;

Fig. 2 Geological map of the study area, with springs and wells studied at the foot of the L'Hajeb Causse (East) and Guigo Causse (West; adapted from Qarqori 2015). Lias limestones behave as aquifers. Triassic clays behave as aquitards. Springs: 1, Bittit; 2, Aguemgam; 3, Ribaa; 4, Sbaa; 5, El Mir; 6, Boucharmou; 7, Bou Youssef; 8, Khadem; 9, Maarouf 1; 10, Maarouf 2. Wells: A, Haj Kaddour (deep well in Saïs Plain); B, Palaeozoic schist well; C, Basaltic schist well

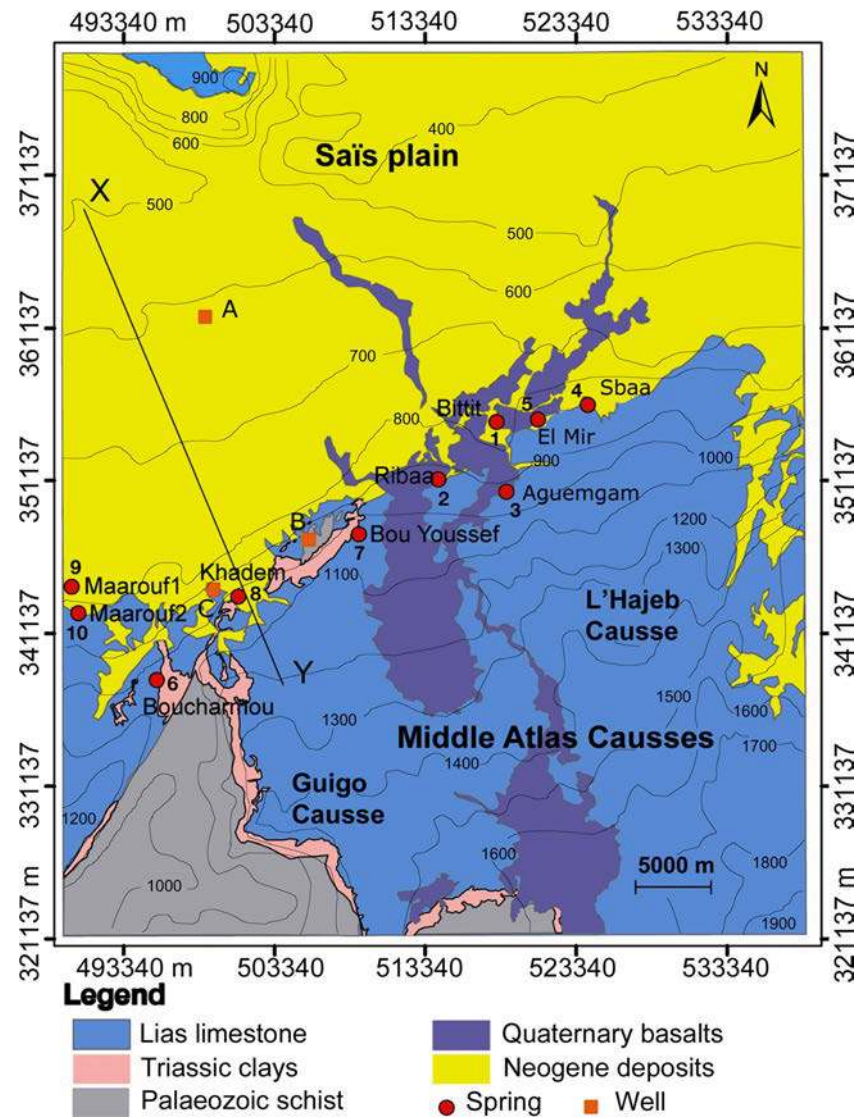
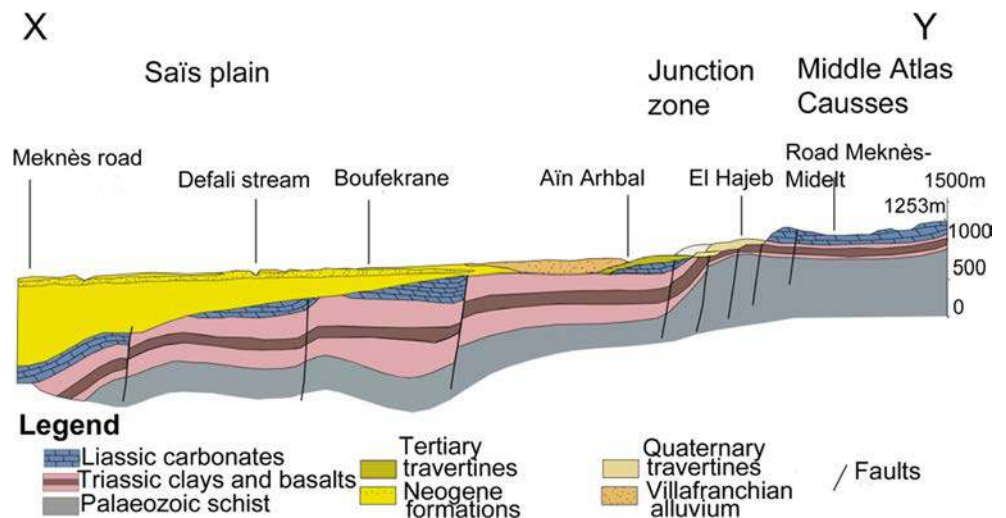


Fig. 3 Geological section (XY, Fig. 2) of the south rifain groove according to the geological map of El Hajeb 1:100,000 (Chamayou et al. 1975)



Khadem; Maarouf 1; Maarouf 2, while the three water wells studied were Haj Kaddour, a deep well (700 m) drawing from a Lias carbonate aquifer in Saïs Plain; a shallow well drawing from Palaeozoic schist (Palaeozoic schist well); and a shallow well in the Basalt-schist environment (Basaltic schist well). After a recall of climatic and hydrogeological context, the results of hydrochemistry analyses (major elements and isotopes) are presented. The interpretation is followed by the building of a schematic model of flow paths, and then by conclusions and perspectives.

Climatic and hydrogeological context

Climatic context

The junction zone of TMA and the study area is characterized by a temperate climate. The TMA is characterized by low temperature compared to the surrounding regions and has a rainfall average of about 730 mm/year (Bentayeb and Leclerc 1977). In winter, the rainfall is enhanced by a frequent west wind with high moisture, whereas at the east of the junction, the climate is dominated by hot and dry winds, the so-called “Sirocco” wind, which can produce more dry summers in TMA.

The Saïs basin is generally characterized by mild winters with average rainfall of about 500–600 mm/year (Chamayou et al. 1975; Agence du bassin hydraulique de Sebou-Fes, 2008–2011). This climate regime is also characterized by relatively constant temperature across the entire Saïs basin, which becomes slightly higher in the east.

During the past 50 years, the frequency of drought periods has increased (Esper et al. 2007; Damnati et al. 2012). In particular, the climate type has become humid to sub-humid in the Ifrane catchment in TMA—altitude 1,635 m above sea level (asl). Using calculations from about 30 years (1980–2010) of meteorological data, the authors of this study observed a drop of the annual rainfall by 17% and an increase of the temperature of the same order in comparison with the period 1933–1963 described in Bentayeb and Leclerc (1977).

Hydrogeological context

The Liassic carbonates outcropping in the TMA are sometimes intercalated with clay layers, thereby forming several local aquifers within the same hydrosystem. At the junction zone, in the Saïs basin, these carbonates are confined by thick Miocene marls, forming an aquifer which is intensively exploited for drinking water and for irrigation. The average water flux of all TMA aquifers is estimated at about 32–35 m³/s, with 10 m³/s transiting to the subterranean Saïs basin (Bentayeb and Leclerc 1977). The flow rate of Bittit spring is from 1.3 to 1.5 m³/s. The flow of Ribaa spring is from 0.02 to 0.32 m³/s and that of Aguemguam spring is typical of a karst

system, from 0 after a dry period to 0.53 m³/s (Agence du bassin hydraulique de Sebou-Fes 2008–2011). During this study (2009–2011) there was an excess of rainwater compared to the normal value of 550 mm in Saïs Plain; the excess was 5% at the end of the study and 47% at the beginning in 2009. Despite this, the water table at Fez-Meknes experienced a piezometric level drop of about 5 m/year, showing a high stress of the system.

The granular porosity of Liassic limestone is low; therefore, the permeability of the matrix is mostly controlled by fractures and karstification. In karst areas it is assumed that about 30% of rainwater recharges groundwater (Drogue 1969; De Jong et al. 2008).

In the junction zone, several important springs of high water quality occur in the northernmost outcrops of Liassic limestone, which is overlain in some areas by Quaternary travertines. Two of these springs in particular, Bittit and Ribaa, almost exclusively provide the drinking water supply for Meknes and the surrounding villages (1.6 million inhabitants), as well as for agriculture. These springs experienced a significant drop in flow rate in the last decades. Although this water originates certainly in the Liassic karst formation, the drop in water table raises several questions regarding the mechanisms of water transport (influence of fractured and karst systems in particular) and the participation of other unknown groundwater reservoirs in the system, which could potentially cause deterioration of groundwater quality. Since 1994–1995, the karst water has suffered from occasional turbidity problems (Amraoui et al. 2003).

Hydrochemistry: methods, results and discussion

Materials and methods

Water samples were taken from springs along the junction between Saïs plain and TMA along the NE–SW section, for both hydrochemical and isotopic analyses. Well-water samples characterize geological structures in the TMA and Saïs plain. Temperature, pH and electrical conductivity were measured in the field. Water samples were collected from springs by rinsing the bottle at least three times and filling it completely before capping, while water samples from wells were collected with a pump after a minimum of several hours pumping. The geochemical characterization of major (Ca²⁺, Mg²⁺, Na⁺, K⁺, Si⁴⁺, Cl⁻, SO₄²⁻, NO₃⁻, HCO₃⁻) and minor (Sr²⁺, Ba²⁺) solutes was done at the Chemical Services of CEREGE by inductively coupled plasma emission spectrometry (Horiba Jobin-Yvon ICP-OES) for major and minor cations, and by capillary electrophoresis (Waters) for anions, from samples collected at the end of the dry and wet season (Table 1; Figs. 4, 5 and 6).

Saturation Indexes for phases in solution were determined by PHREEQC version 2.7 (Parkhurst and Appelo 1999) with database wateq.dat—Table S1 in the electronic supplementary

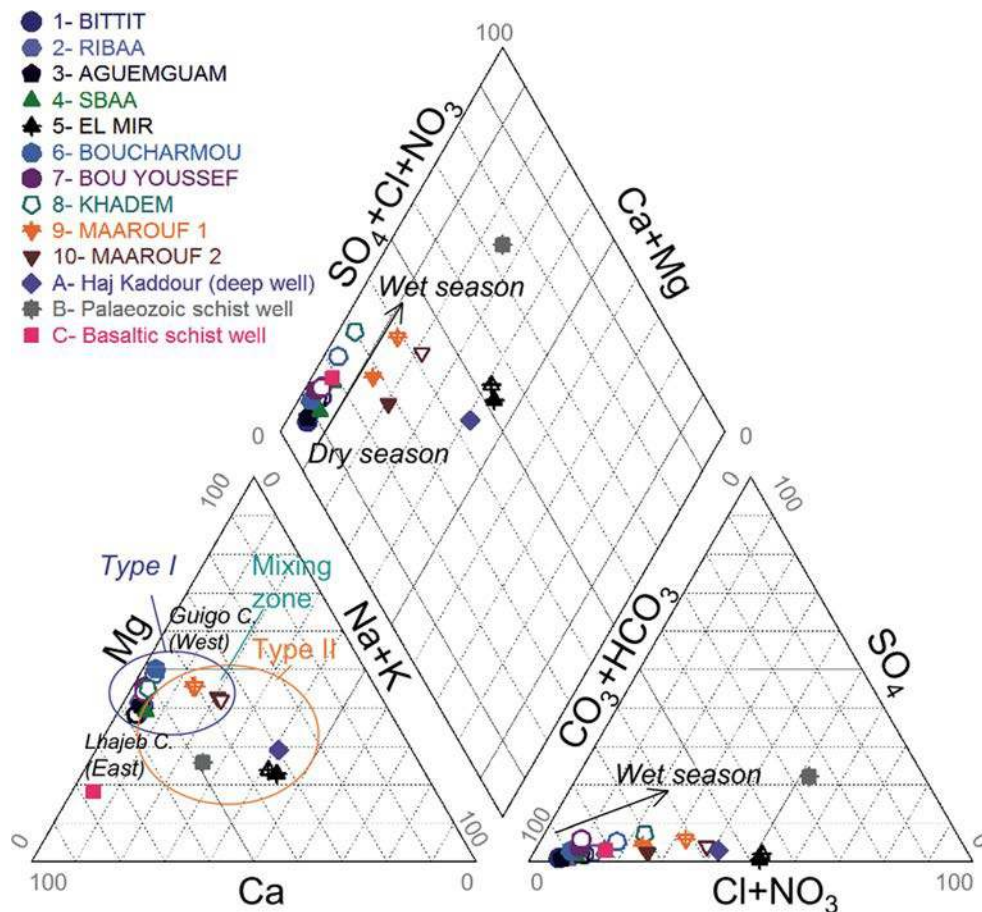
Table 1 Chemical data of springs and wells for the sampling campaigns (2009–2010)

Code: name (spring or well)	Sample number	Sample date	Water type	Geological area	Alt. Z (m asl)	Temp (°C)	EC (µS/cm)	pH	Ca ²⁺ (mg/L)	Mg ²⁺ (mg/L)	Na ⁺ (mg/L)	K ⁺ (mg/L)	ST ⁺ (mg/L)	Si ²⁺ (µg/L)	Ba ²⁺ (µg/L)	Cl ⁻ (mg/L)	SO ₄ ²⁻ (mg/L)	NO ₃ ⁻ (mg/L)	HCO ₃ ⁻ (mg/L)
1: Btiti spring	1.1	Oct. 2009	I	Lhajeb C.	775	16.8	591	7.18	69.7	31.3	6.33	0.89	4.36	43.97	3.59	9.49	3.19	12.2	405
	1.2	March 2010				16.5	555	7.45	68.3	27.9	5.77	1.12	4.95	ND	ND	9.06	4.20	16.1	234
	1.3	Oct.–Nov. 2010				16.4	580	7.50	68.6	31.1	5.42	0.85	4.93	50.20	4.25	10.1	3.72	17.5	268
2: Ribaa spring	2.1	Oct. 2009	I	Lhajeb C.	937	16.6	588	7.67	70.0	31.8	6.25	0.82	4.65	43.95	3.60	9.90	3.25	13.9	317
	2.2	March 2010				16.9	565	7.88	67.6	30.5	4.32	0.97	5.52	ND	ND	6.91	4.79	26.2	237
	2.3	Oct.–Nov. 2010				16	583	7.49	72.8	31.1	5.21	1.91	4.94	52.01	5.32	8.65	3.12	15.0	284
3: Aguenguam spring	3.1	Oct. 2009	I	Lhajeb C.	919	16.3	590	7.22	71.2	32.1	5.87	0.86	4.47	43.83	3.00	9.53	3.11	12.4	375
	3.2	March 2010				15.9	559	7.33	70.5	28.4	5.27	1.18	6.31	ND	ND	8.47	4.12	16.4	246
	3.3	Oct.–Nov. 2010				15.8	548	7.54	68.8	31.0	5.22	0.87	4.80	48.35	4.15	7.58	2.91	13.9	271
4: Shaa spring	4.1	Oct. 2009	II	Lhajeb C.	855	18.7	678	7.15	81.3	35.2	10.2	0.89	3.24	39.64	3.98	16.7	5.19	13.5	370
	4.2	March 2010				18.9	661	7.13	77.2	34.1	8.10	1.49	2.55	ND	ND	17.0	7.30	23.8	275
	4.3	Oct.–Nov. 2010				18.5	638	7.30	80.7	35.1	9.65	1.81	3.21	43.16	5.85	16.6	5.15	15.8	319
5: El Mir spring	5.1	Oct. 2009	II	Lhajeb C.	840	19	1,232	7.09	79.1	32.5	118	1.99	5.71	97.88	3.66	186	3.07	11.1	306
	5.2	March 2010				18.5	1,086	7.16	76.1	31.3	102	1.89	5.78	ND	ND	154	8.67	20.3	257
	5.3	Oct.–Nov. 2010				18.4	1,276	7.40	78.9	32.5	1.29	2.64	5.63	105.4	5.50	215	6.95	12.6	264
6: Boucharmou spring	6.1	Oct. 2009	I	Guigo C.	1,041	19.1	529	7.46	53.5	34.7	3.18	0.91	2.40	42.45	2.34	6.49	9.89	23.6	384
	6.2	March 2010				18.7	517	7.97	53.9	34.3	3.50	1.06	2.32	ND	ND	10.5	11.2	27.9	204
7: Bou Youssef spring	7.1	Oct. 2009	I	Guigo C.	1,059	18.3	551	7.41	63.2	33.6	3.11	0.93	2.10	32.72	3.15	6.84	10.6	24.8	320
	7.2	March 2010				17.4	528	7.58	60.0	30.6	3.64	1.62	2.38	ND	ND	6.60	11.5	11.5	212
8: Khadem spring (El Hajeb)	8	March 2010	I (?)	Guigo C.	1,017	17.7	578	7.52	64.0	33.7	4.60	1.13	2.23	ND	ND	9.07	16.4	52.3	207
9: Maarouf 1 spring	9.1	Oct. 2009	II	Guigo C.	781	20.1	701	7.27	59.7	40.4	22.3	1.17	3.17	56.01	5.12	39.5	14.4	37.9	320
	9.2	March 2010				20.1	698	7.38	58.1	39.6	22.7	1.16	2.78	ND	ND	43.7	16.4	41.3	218
10: Maarouf 2 spring	10.1	Oct. 2009	II	Guigo C.	853	20.1	751	7.27	56.9	40.1	35.2	2.23	3.05	51.26	4.91	59.1	9.26	28.2	364
	10.2	March 2010				20.2	759	7.42	55.5	39.0	35.4	4.52	2.90	ND	ND	63.7	12.0	39.9	225
A: Haj Kaddour (deep well in Saïs)	A	Oct. 2009	II	Saïs Plain	644	26.6	991	7.31	56.2	33.3	88.7	1.13	3.82	93.92	7.36	130	12.2	10.1	315
B: Palaeozoic schist well	B.1	Oct. 2009	III	Guigo C.	977	20	1,210	7.81	112.5	36.0	64.0	6.78	6.69	599.8	29.25	140	115	106	170
	B.2	Oct.–Nov. 2010				ND	ND	ND	222.7	43.8	41.8	4.85	6.70	479.0	26.40	192	122	289	142
C: Basaltic schist well	C	Oct. 2009	III	Guigo C.	912	18.3	530	7.52	88.3	12.5	5.60	1.36	6.23	42.20	7.36	11.4	7.65	36.0	279

Site codes for the sampling campaigns (2009–2010). Springs and wells are referenced as in Fig. 2. Springs: 1, Btiti; 2, Aguenguam; 3, Ribaa; 4, Shaa; 5, El Mir; 6, Boucharmou; 7, Bou Youssef; 8, Khadem; 9, Maarouf 1; 10, Maarouf 2. Wells: A, Haj Kaddour (deep well in Saïs Plain); B, Palaeozoic schist well; C, Basaltic schist well. Sample numbers are shown in principal component analysis (PCA)

C. Causee; ND not determined

Fig. 4 Piper diagram showing water geochemistry of springs and wells. Springs and wells are referenced as in Fig. 2. Characterization of two types of waters from Liassic and Triassic origins, including two Liassic aquifers, in the north-eastern sector (L'Hajeb Causse) and south-western sector (Guigo Causse). The effect of seasonality is mainly shown by sulfates and chlorides. Solid symbols represent dry season, and open symbols represent wet season. Note: This figure was derived using "Diagrammes" software V. 5.9 (Simler 2012)



material (ESM). Stable isotopes ($\delta^{18}O$, δD) were measured at the Geochemical Laboratory of the Faculty of Science at the University of Avignon (France) by mass spectrometry. Stable isotopes were analyzed in spring and well water samples collected during the four sampling campaigns (Table 2; Fig. 7).

Radon activities in groundwater were measured via ^{218}Po counting using a RAD7 alpha spectrometer. Water samples had been collected using an immersion pump providing a constant water flow rate of 3.5 L/min into 250-ml glass bottles. In order to minimize radon degassing, the volumes of the bottles were displaced twice during continuous flow (Fig. 8).

To specify the types of waters and the mixing zones, multivariate statistical analysis of the data was performed (Tables 3 and 4; Fig. 9) with an Excel application (Georgin 2007). Principal component analysis (PCA) was carried out on 25 individual samples (24 samples from springs and 1 sample from well A) for 11 variables (geochemical parameters and radon) listed in Tables 1 and 2. Wells B and C, which were polluted by human activity, were not taken into account.

Major element geochemistry

The analyses allow characterization of the water–rock interactions in the aquifers (Figs. 4, 5 and 6; Table 1). Figures 4, 5, 6

and 8 were developed using "Diagrammes" software V. 5.9 (Simler 2012). All collected spring waters are calcium and magnesium bicarbonate waters. Speciation of these waters, calculated using PHREEQC version 2.7, indicates saturation conditions (see Table S1 of the ESM) with respect to calcite and dolomite for all springs and wells. A clear distinction among three groundwater types can be based on Ca^{2+} , Mg^{2+} , Na^+ , K^+ , Cl^- and SO_4^{2-} . Type I comprises calcium-magnesium bicarbonate waters collected in the southern sectors: Bittit (site 1), Ribaa (site 2), Aguemguam (site 3), Boucharmou (site 6), Bou Youssef (site 7), and Khadem (site 8). These waters are characterized by variable Mg/Ca ratios, indicating dissolution of limestone and dolomite in the aquifer to various extents (Fig. 6). Some of them, notably Boucharmou, have a Mg/Ca ratio of nearly one, indicative of pure dolomite dissolution. Type II waters—Sbaa (site 4), El Mir (site 5), Maarouf 1 (site 9), Maarouf 2 (site 10), and the deep well (A) Haj Kaddour 2360/15 in Saïis Plain—includes waters characterized by a clear enrichment in Na^+ and Cl^- , with a slightly lower Mg/Ca, compared to type I.

Dolomite— $\log K_s = -16.54$ at 25 °C (K_s : solubility product)—is less soluble than calcite ($\log K_s = -8.48$ at 25 °C) and can hardly reprecipitate (Michalowski and Asuero 2012); thus, the Mg/Ca values between 1 and 1.1 in the western sector in type I springs seem to be a consequence of a more

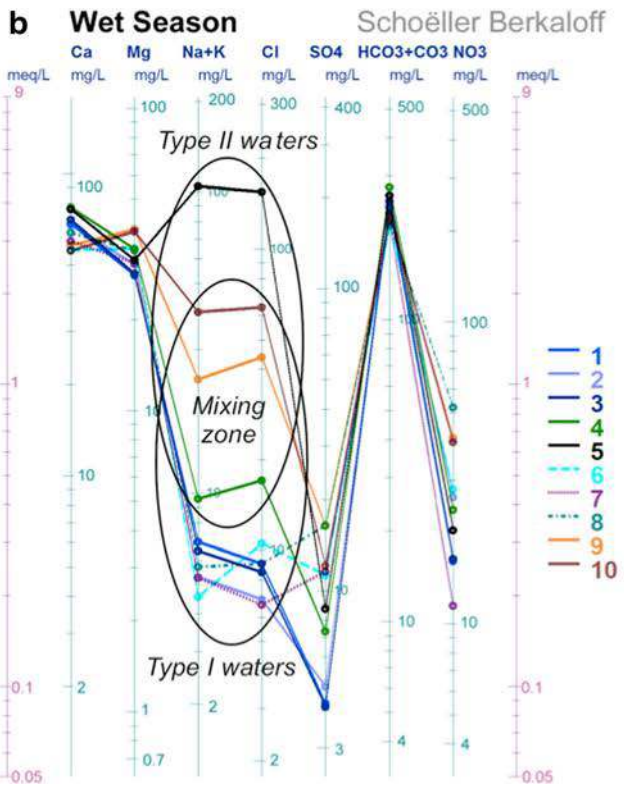
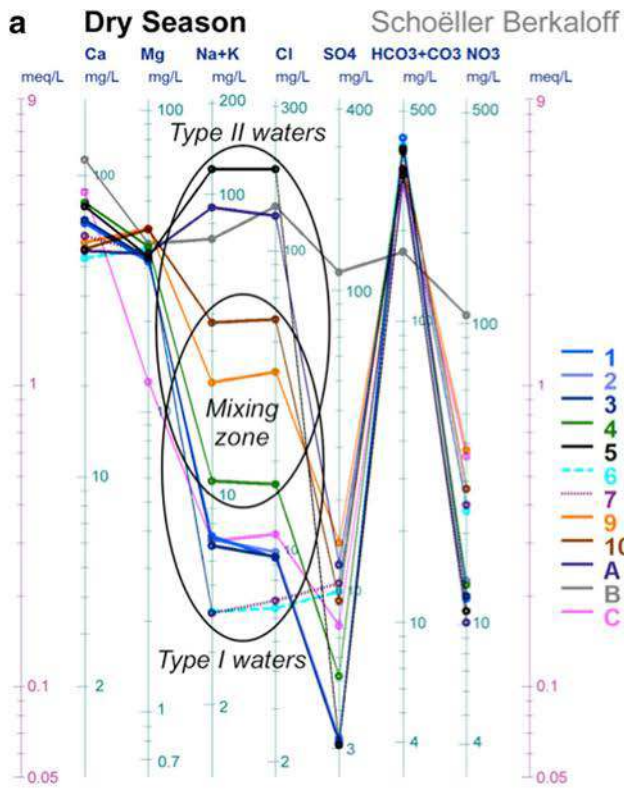


Fig. 5 Seasonality expressed by Schoeller-Berkaloff diagrams, in a dry season (October–November) and **b** wet season (March–April). Sites are referenced as in Fig. 2. Types of spring waters and mixing zones for the eastern and the western sectors are shown. Note: This figure was derived using “Diagrammes” software V. 5.9 (Simler 2012)

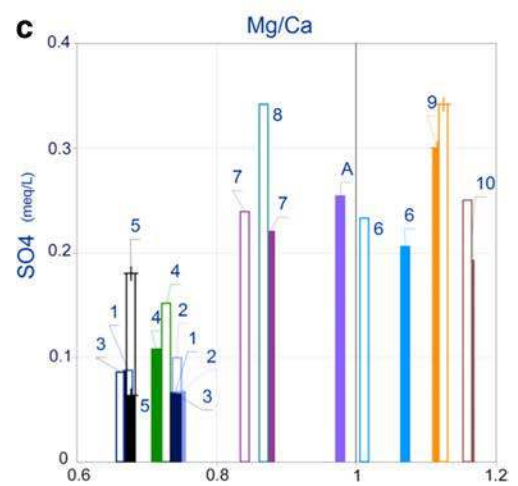
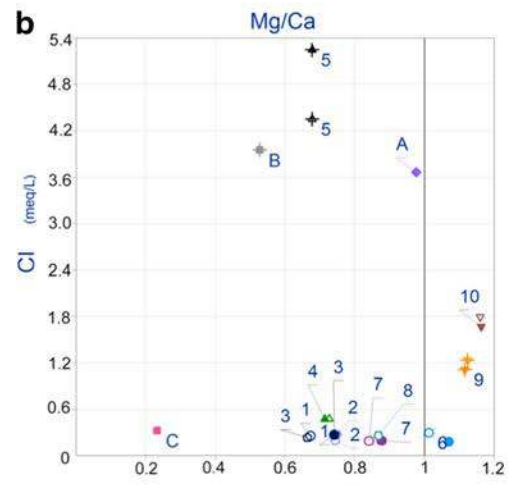
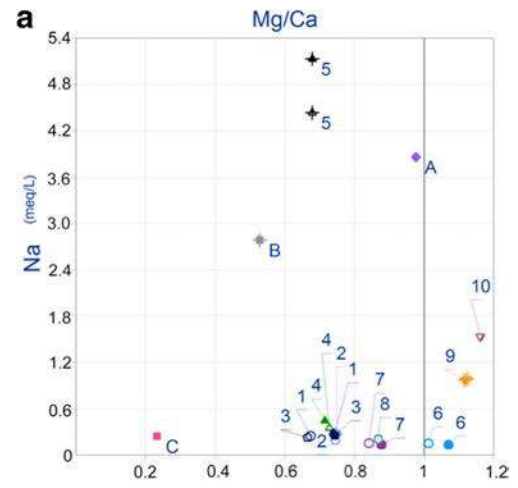


Fig. 6 Mg/Ca ratio as an indicator of limestone and dolomite dissolution versus **a** sodium, **b** chloride and **c** histogram of sulfates, showing seasonality. Mg/Ca < 1: L’Hajeb Causse. Mg/Ca ≤ 1.1: Guigo Causse. Springs and wells are referenced as in Fig. 2. Note: This figure was derived using “Diagrammes” software V. 5.9 (Simler 2012)

advanced dissolution of the dolomite component of the aquifer with waters having longer transit times.

Type III is represented by well B drilled in the Palaeozoic schist formation (Palaeozoic schist well) and by well C drilled

Table 2 Isotopic data of springs and wells, d: deuterium excess ($d = \delta D - 8 \times \delta^{18}O$), for the four sampling campaigns (2009–2011) with some values of Feb. 2007 (El Ouali et al. 2014)

Code: name (spring or well)	Water type	Sample date	$\delta^{18}O$ (V. VSMOW)‰	δ^2H (V. VSMOW)‰	d ‰	^{222}Rn (Bq/m ³)	SD ^{222}Rn (Bq/m ³)	Z_{rech} (m asl)
1: Bittit spring	I	Feb. 2007	-7.65	-42.87	18.3	–	–	1,415
		Oct. 2009	-7.58	-48.82	11.8	3,330	383	
		March 2010	-7.40	-44.23	15.0	4,320	436	
		Oct.–Nov. 2010	-7.39	-44.73	14.4	–	–	
		Nov. 2011	-7.58	-45.55	15.1	–	–	
2: Ribaa spring	I	Feb. 2007	-7.42	-42.68	16.7	–	–	1,391
		Oct. 2009	-7.54	-48.21	12.1	1,976	295	
		March 2010	-7.17	-42.58	14.8	3,820	410	
		Oct.–Nov. 2010	-7.58	-46.47	14.2	–	–	
		Nov. 2011	-7.57	-45.39	15.2	–	–	
3: Aguemguam spring	I	Oct. 2009	-7.60	-48.80	12.0	2,137	307	1,435
		March 2010	-7.51	-43.87	16.2	3,458	390	
		Oct.–Nov. 2010	-7.57	-45.86	14.7	–	–	
		Nov. 2011	-7.61	-46.1	14.8	–	–	
4: Sbaa spring	II	Oct. 2009	-6.93	-44.92	10.5	10,753	688	1,185
		March 2010	-6.78	-39.94	14.3	9,640	651	
		Oct.–Nov. 2010	-6.92	-42.71	12.7	–	–	
		Nov. 2011	-6.97	-42.02	13.7	–	–	
5: El Mir spring	II	Oct. 2009	-6.42	-42.08	9.3	12,894	753	1,063
		March 2010	-6.60	-39.54	13.3	16,464	851	
		Oct.–Nov. 2010	-6.50	-40.59	11.4	–	–	
		Nov. 2011	-6.76	-41.64	12.4	–	–	
6: Boucharmou spring	I	Oct. 2009	-6.54	-43.73	8.6	4,656	453	1,042
		March 2010	-6.49	-41.01	10.9	4,267	433	
7: Bou Youssef spring	I	Oct. 2009	-6.40	-41.35	9.9	4,351	437	997
		March 2010	-6.40	-38.09	13.1	2,597	338	
		Nov. 2011	-6.37	-38.32	12.6	–	–	
8: Khadem spring (El Hajeb)	I (?)	March 2010	-6.65	-41.03	12.2	5,623	497	1,093
9: Maarouf 1 spring	II	Oct. 2009	-5.90	-40.67	6.5	7,960	592	846
		March 2010	-6.07	-38.82	9.7	5,511	492	
10: Maarouf 2 spring	II	Feb. 2007	-6.16	-37.51	11.8	–	–	927
		Oct. 2009	-6.18	-42.15	7.3	3,043	366	
		March 2010	-6.16	-38.30	11.0	2,776	349	
		Nov. 2011	-6.31	-40.26	10.2	–	–	
A: Haj Kaddour (deep well in Saïs)	II	Oct. 2009	-6.20	-40.69	8.9	3,227	377	981
		Nov. 2011	-6.50	-40.69	11.3	–	–	
B: Palaeozoic schist well	III	Oct. 2009	-5.44	-35.14	8.3	263.5	108	609
		Nov. 2011	-5.25	-33.66	8.3	–	–	
C: Basaltic schist well	III	Oct. 2009	-5.88	-37.79	9.3	1,120	222	807

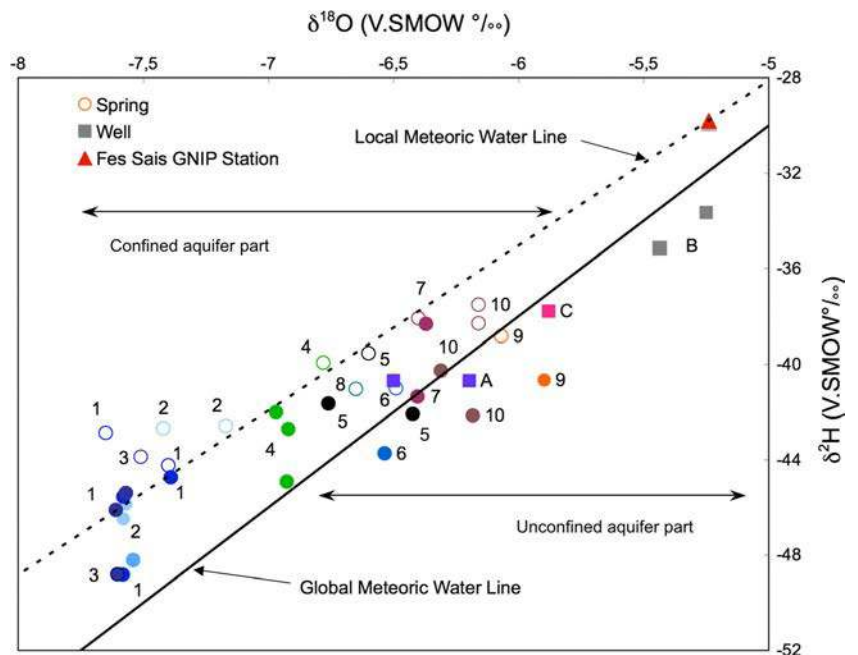
The main elevation of recharge zone is obtained as follow: $Z_{rech} (m) = -(\delta^{18}O + 3.7)/0.27$ (Sefrioui et al. 2010). Stable isotopes are expressed versus VSMOW (Vienna Standard Mean Ocean Water)

SD ^{222}Rn standard deviation for radon

in the Tertiary basalts (Basaltic schist well). Both of them are characterized by a high level of sulfate and low Mg/Ca ratio compared to type II. One can distinguish well B from well C by Na and Cl values that are high for B and lower for C (Table 1; Fig. 6). These two water samples are however clearly

polluted by nitrate (probably recent anthropogenic pollution); hence, their chemistry cannot be taken as representative of an equilibrium condition for the Palaeozoic schist or the Tertiary basalts. Saturation conditions for anhydrite, gypsum and barite are not reached in any of these waters for the data set.

Fig. 7 Seasonality and geographical origin of springs and wells are displayed from stable isotopes ($\delta^{18}\text{O}$, $\delta^2\text{H}$) data with respect to the global meteoric water line (black line; Rozanski et al. 1993) and local meteoric water line (dashed line; El Ouali et al. 2014). A confined aquifer is characterized in the eastern sector (L'Hajeb Causse) and an unconfined aquifer in the western sector (Guigo Causse). Solid symbols represent dry season for October–November (2009–2011), and open symbols represent wet season for February–April (this study, 2010–2011) and some values for February 2007 of El Ouali et al. (2014)



Isotopic analyses ($\delta^{18}\text{O}$, δD) and altitudes of recharge zones

The results of analyses are compared to the global meteoric water line (GMWL; Rozanski et al. 1993) and the local meteoric water line (LMWL), which has the following formula (El Ouali et al. 2014): $\delta\text{D} = 6.9 \times \delta^{18}\text{O} + 6.4$. Isotopic values have the ranges:

$-7.65\text{‰} < \delta^{18}\text{O} < -5.25\text{‰}$ and $-48.82\text{‰} < \delta^2\text{H} < -33.66\text{‰}$. Two groups of groundwaters co-exist according to their geographical origin. Water samples of the northeast sector around Bittit (L'Hajeb Causse) have a less-enriched isotopic composition and correspond to a confined aquifer, while samples of the southwest sector (Guigo Causse) correspond to groundwater with a high evaporation component (less confined); furthermore,

Fig. 8 Electrical conductivity (EC) of water versus ^{222}Rn activity and transit time of water from the Triassic aquitard to the Liassic aquifer. Springs and wells are referenced as in Fig. 2. Note: This figure was derived using “Diagrammes” software V. 5.9 (Simler 2012)

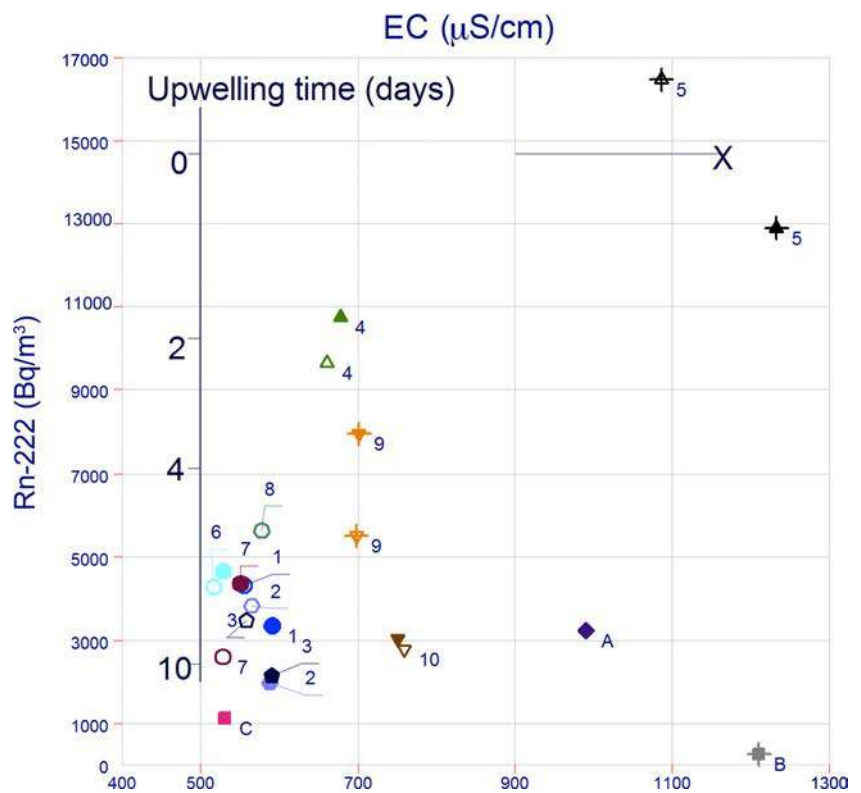


Table 3 Correlation matrix between geochemical parameters (see Table 1) and radon (Rn, see Table 2) for the 25 individual components of springs considered (1.1–10.2) and well A

Correlation	EC	Ca ²⁺	Mg ²⁺	Na ⁺	K ⁺	Si ⁴⁺	Cl ⁻	SO ₄ ²⁻	NO ₃ ⁻	HCO ₃ ⁻	Rn
EC	1	0.319	0.116	0.989	0.462	0.383	0.991	0.035	-0.180	0.020	0.656
Ca ²⁺		1	-0.417	0.240	-0.039	0.536	0.234	-0.661	-0.500	0.150	0.594
Mg ²⁺			1	0.058	0.353	-0.609	0.090	0.631	0.615	0.166	0.035
Na ⁺				1	0.442	0.399	0.997	0.056	-0.201	0.022	0.597
K ⁺					1	-0.005	0.471	0.170	0.202	0.242	0.066
Si ⁴⁺						1	0.380	-0.687	-0.521	0.026	0.231
Cl ⁻							1	0.073	-0.171	0.037	0.600
SO ₄ ²⁻								1	0.760	0.342	-0.037
NO ₃ ⁻									1	0.385	-0.024
HCO ₃ ⁻										1	-0.012
Rn											1

a seasonal effect for springs is observed between the end of the dry season in autumn (solid circles in Fig. 7) and the end of the wet season in March (open circles in Fig. 7).

The deuterium excess is defined by $d_{\text{excess}} = \delta D - 8 \times \delta^{18}\text{O}$ (Dansgaard 1964; Craig and Gordon 1965). A higher deuterium excess (see Table 2) characterizes all spring waters with respect to the local meteoric water line ($d_{\text{excess}} < 8$). This is particularly evident for samples collected after the rainy season—March/April 2010; Fig. 7 (open circles), see values in Table 2. This shift indicates a larger kinetic effect in the vapor source region for the winter recharge. Spring waters of type I have slightly lighter isotopic compositions than waters of type II. This difference most likely reflects a higher altitude of the recharge area for spring waters of type I, compared to spring waters of type II.

Moreover, it was observed that springs of water type I in the northeastern part (complex Ribaa-Bittit) have some isotopic compositions lower than springs of the same type in the southwestern part, which corresponds to higher recharge altitudes for the northeast. These altitudes (Sefrioui et al. 2010) correspond to values of vertical gradient for $\delta^{18}\text{O}$ of -0.27‰ per 100 m of rise and they are estimated for the studied area (in

Table 4 Eigenvalues and percentage of total inertia of the PCA

Axis	Eigenvalue	Total inertia
Axis 1	4.151	41.5%
Axis 2	2.957	29.6%
Axis 3	1.231	12.3%
Axis 4	0.891	8.9%
Axis 5	0.386	3.9%
Axis 6	0.213	2.1%
Axis 7	0.107	1.1%
Axis 8	0.061	0.6%
Axis 9	0.002	0.0%
Axis 10	0.001	0.0%

m asl) following the formula $Z_{\text{recharge}} = -(\delta^{18}\text{O} + 3.7)/0.27$ (El Ouali et al. 2014; Table 2).

The Liassic aquifer has recharge areas located at $\sim 1,400$ m asl in the eastern sector (L'Hajeb Causse) and at $\sim 1,000$ m asl in the western sector (Guigo Causse). Waters in contact with the Triassic aquitard (El Mir spring) in the eastern sector are recharged around 1,000 m asl and the two mixed zones are highlighted at the ends of the basin: one corresponds to Sbaa spring with an intermediate recharge area ($\sim 1,200$ m asl); the second to Maarouf spring with a more local recharge area (900 m asl; see Table 2), showing a net distinction between the eastern and western sectors. There is evidence of a drain (or preferential flow) of waters perpendicular to the Causes in the Bittit-Ribaa area, which could be confirmed with geophysical investigations.

Transit times from radon activity and tritium constraints

Radon activity and transit time

Radon measurements (Table 2; Fig. 8) have been calibrated from B, the Palaeozoic schist well, in contact with the Triassic aquitard, to obtain the high limit of electrical conductivity. Type I waters in the Liassic aquifer yield a mean radon activity of about 3,500 Bq/m³, which is probably resulting from secular equilibrium with the aquifer carbonates. This level of activity is typical for fresh groundwater in Mesozoic carbonate formations (Savoy et al. 2011). The steady-state radon is achieved when the rate of radon disintegration matches the rate of radon generation supported by the decay of the parent isotope, ²²⁶Ra, present in the aquifer material (Hoehn and Von Gunten 1989). Radon sources in karstic waters are the radium in limestone (due to trace concentration of uranium in calcite) and deposits of “terra rossa”, which contain clays minerals, Al-Fe-Mn hydroxides and organic matter that may accumulate radium (Tadolini and Spizzico 1998). Once the

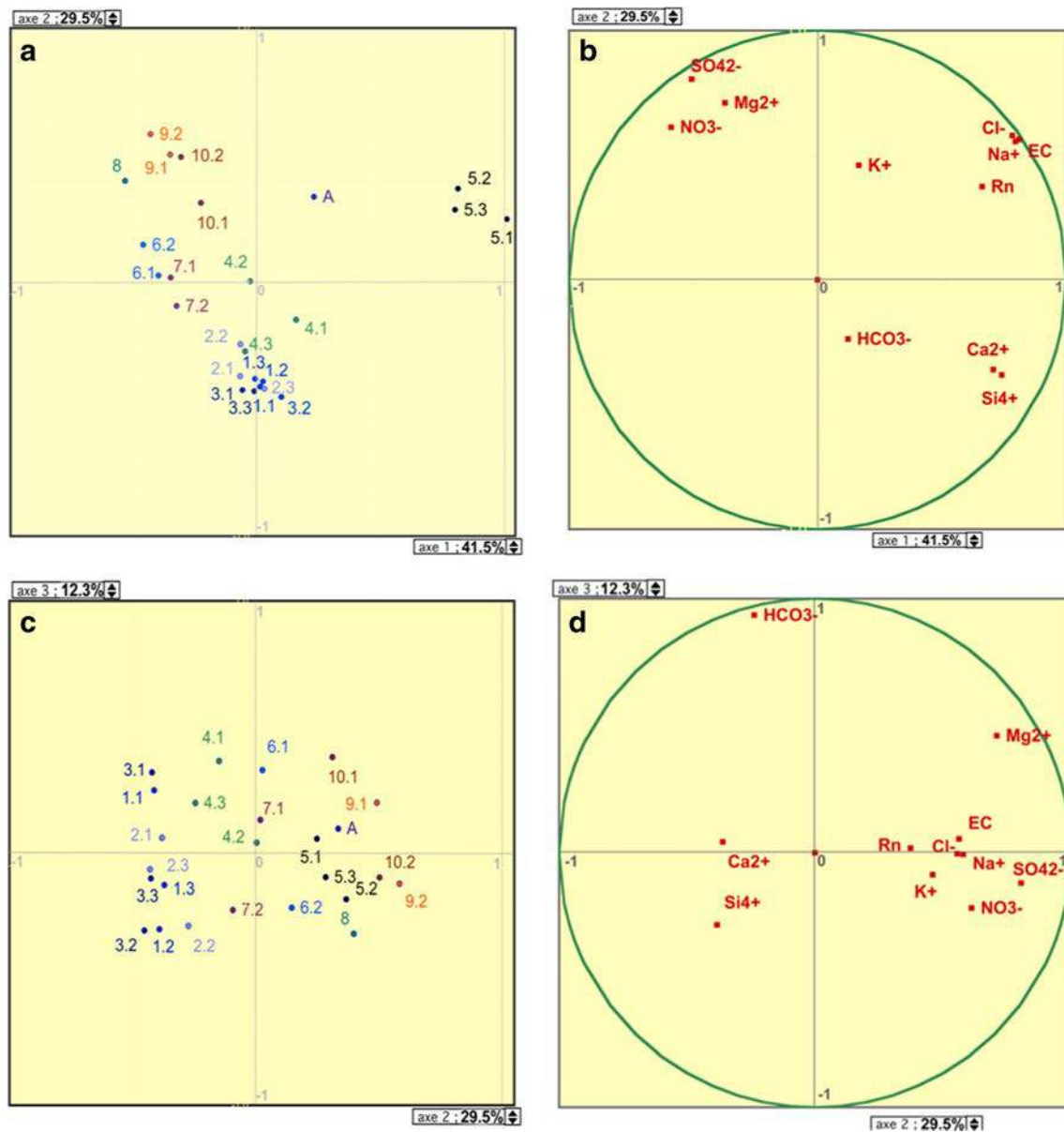


Fig. 9 Principal component analysis (PCA) representations of individuals (25 samples of water) (a–c) and variables (chemical parameters) (b–d). Main plane (71.1% of inertia) defined by axes 1 and 2 (a–b). Second plane (41.8% of inertia) defined by axes 2 and 3 (c–d). **a** Five sub-populations of groundwater are identified in the main planes 1 and 2. Axis 1 discriminates the set of (i) [Bittit, Ribaa, Aguemguam (1.1–3.3)] from (ii) [El Mir (5.1–5.3), Haj Kaddour (A)] and from (iii) [Maarouf 1 and 2 (9.1–0.2), Khadem (8)]. Axis 2 discriminates (iii)

[Maarouf, Khadem], (iv) [Boucharmou and Bou Youssef (6.1–7.2)] from (ii) [El Mir, Haj Kaddour]. (v) Sbaa (4.1–4.3) is a typical mixing zone (origin of axis). **b** Geochemical elements in plane 1 and 2. Axis 1 explains Cl^- , Na^+ , EC, Si^{4+} , Ca^{2+} ; axis 2 explains SO_4^{2-} , Mg^{2+} , NO_3^- . **c** Springs and well in plane 2 and 3. Axis 3 discriminates [Bittit, Ribaa, Aguemguam (1.1–3.3)] from Maarouf 1 and 2 (9.1–10.2). **d** Geochemical elements in planes 2 and 3. Axis 2 explains Mg^{2+} and SO_4^{2-} ; Axis 3 explains HCO_3^-

radon steady state is reached (around three half-lives, i.e. 12 days) no information about transit time is obtainable from radon. The transit time of these waters from the recharge zone to the spring is thus more than 12 days. The differences in the altitude of springs do not lead to any significant radon variations, so it is not possible to highlight shorter transit times for the higher altitude springs based on radon activity. However, two kinds of aquifers for this group are noted, as previously seen in isotopic analyses ($\delta^{18}\text{O}$, δD): one in the eastern sector

correlated to the seasonal variations (around $3,200 \pm 450 \text{ Bq/m}^3$), the other in the western sector that seems constant around $5,000 \text{ Bq/m}^3$.

Type II waters are characterized by significantly higher ^{222}Rn activity, reaching a mean value of $15,000$ with a seasonality of $\pm 1,000 \text{ Bq/m}^3$. To explain this higher radon activity compared to type I, a possibility is that these groundwaters are in equilibrium with an aquifer containing higher radium concentrations.

The radium concentration in the Liassic aquifer (Savoy et al. 2011) is constantly independent of the two groups of water. Besides, there is no reason to think that the higher activity results from lesser degassing compared to type I. Therefore, it is assumed that the higher radon activity of waters of type II results from interactions with the Triassic evaporites at the base of the Lias. Moreover, this interpretation is supported by the enrichment in sulfate and chloride, which indicates an interaction with gypsum and halite, typically found in Triassic evaporites of the area. The enrichment in radon activity is specific for groundwater having a higher content in sulfate, because radium typically co-precipitates in the aquifer together with barite and other insoluble sulfates (Rosenberg et al. 2013), which constitute a permanent radon source in the aquifer. Since Triassic formations in the area behave as aquitards (they essentially consist of low-permeability evaporites and schist with few carbonates), one cannot consider a true Triassic evaporite aquifer, but rather an interaction-zone between carbonates and evaporites, located near the base of Liassic dolomitic limestone.

The two samples of the El Mir spring showing the larger enrichments in Na and Cl indicate that these waters interact the most with the evaporites of the Permo-Triassic sequence; furthermore these springs have elevated radon activity and a similar chloride to the water directly extracted from the Palaeozoic schist well (Figs. 6a–c and Fig. 8; Table 2). One may assume that the radon secular equilibrium activity in the interaction zone with the Permo-Triassic basement is equal or higher than 16,000 Bq/m³.

Three springs (Figs. 4, 5, 6, 7 and 8) represented by green (No. 4), orange (No. 9) and brown (No. 10) symbols have geochemical compositions (stable isotopes, major elements) intermediate between type I and type II waters. These spring waters result from a mixing zone between the two groups. Their radon activity is however higher than the expected activity from simple binary mixing (see Fig. 8), indicating that the mixing occurs while waters interact with the Triassic evaporites. The opposite possibility (i.e. mixing is in the Liassic carbonates) can be dismissed since in that case the radon activity would be lower than the values shown by the mixing zone. The excess of radon, with respect to the expected activity of the mixing, depends on the in-growth time of radon in the interaction zone. However, this radon excess declines during the successive transfers to the surface due to the radioactive decay. These waters would ultimately reach the radon secular equilibrium activity of the Liassic limestone (3,500 Bq/m³) on a time scale of 12 days.

In other words, type II waters have the highest measured radon activity and major-element geochemistry most similar to the groundwater extracted from the Triassic schist (well B). If it is assumed that 16,000 Bq/m³ is the secular-equilibrium activity in the mixing zone (Fig. 8), one may assume, for the three intermediate water samples (green No. 4, orange No. 9 and brown No. 10 symbols), the upwelling time since these

waters have left the contact with the Triassic evaporites to enter the Liassic aquifer and reach the surface is thus less than 12 days, on probably on the order of a few days. Remote sensing images of this area point out that these mixed springs or zones lie on important tectonic alignments (Qarqori 2015; Dauteuil et al. 2016), which suggests that a fracture system could play a role in the fast upwelling of groundwater.

Tritium constraints on the recharge areas

It was noted that two types of recent sources of tritium exist (half-life = 12.32 years, from Lucas and Unterweger 2000; ³H ~ 5.0 ± 0.3 TU from IAEA 2010) with a complete recharge in less than 5 years. The groundwater residence time verifies a “piston model” (Hubert and Olive 1995): effective rainfall runs through the karst at a relatively constant velocity, and because the residence time is less than 5 years, the waters have an average age of less than three years in the aquifer. The tritium activity in the eastern sector is slightly weaker than the activity in the western sector; this seems to indicate a quicker recharge for the eastern than for the western sector. These results are in good accordance with the different recharge altitudes obtained with isotopic analyses (δ¹⁸O, δD). In the eastern sector (L’Hajeb Causse), the recharge areas have higher altitudes than in the west (Guigo Causse).

Principal component analysis (PCA) of data and implication for the mixing zones

The correlation matrix (Table 3) shows a strong correlation (>0.9) between Na⁺, Cl⁻ and electrical conductivity (EC), which confirms the dissolution of Triassic halite and a good correlation (0.7; 0.9) for nitrate and sulfate coming from shales of the Triassic aquitard. Moderate correlation (~0.6) between Mg²⁺ and SO₄²⁻ and between Mg²⁺ and NO₃⁻ shows an interaction between the Liassic aquifer mainly composed of dolomitic carbonates and the shale-rich Triassic aquitard. Calcium and silicon are poorly correlated (~0.5), which is consistent with low clay content in the Liassic carbonate aquifer (eastern sector around Bittit). Calcium and sulfate are inversely correlated, which indicates that groundwater chemistry is dominated by dissolution of Liassic carbonates in some areas and of gypsum (from the Triassic aquitard) in others. Si⁴⁺ and Mg²⁺ as well as Si⁴⁺ and SO₄²⁻ are anti-correlated. This seems to indicate that the aquifer rich in magnesium contains very low silicon and probably very low clays. Moreover, the presence of silicon is the mark of a bicarbonate aquifer poor in sulfates. This confirms the existence of two types of aquifers more or less rich in Ca²⁺ and/or Mg²⁺.

From graphical representations of the principal component analysis for individuals and variables (Fig. 9a–d), it is possible to study the factorial planes formed by axes 1, 2 and 3 which

represent a global inertia of 83.4%. These planes are associated with eigenvalues greater than 1 (Table 4).

In the main plane (Fig. 9a), the individuals form five distinct clouds, which means that sub-populations of water have been highlighted. These subpopulations correspond to (1) Maarouf 1 and 2 (9.1–10.2) and Khadem (8); (2) Boucharmou and Bou Youssef (6.1–7.2); (3) Sbaa (4.1–4.3); (4) Bittit, Ribaa, Aguemguam (1.1–3.3); and (5) El Mir (5.1–5.3) and the well A.

The results (Figs. 9a–d) allow the types of water to be specified: for the L'Hajeb Causse in the east, waters of the main Liassic aquifer (Bittit, Ribaa, Aguemguam) are calcium and magnesium bicarbonate with possible dissolved clays. They characterize type I waters. The clay content in waters is low but it explains problems of turbidity after heavy rains. The water represented by El Mir shows high sodium and chloride at a similar concentration to each other and a high radon content characteristic of Triassic aquitards, which characterize type II. Sbaa is just at the origin of axes 1 and 2, i.e. presents no main component. It represents a typical mixing zone between type I and type II waters of the L'Hajeb Causse.

For the Guigo Causse in the west, waters in the Liassic aquifer (Boucharmou, Bou Youssef) are marked by higher magnesium content than those of the L'Hajeb Causse. This is in agreement with a longer transit time. However, these type I waters are weakly marked by nitrate and sulfate, indicating that the Triassic interacts with the Liassic aquifer. This is in accordance with a discontinuous and more faulted structure of the Guigo Causse. Type II waters (Maarouf 1 and Maarouf 2) are marked by their magnesium, nitrate and sulfate content, which confirm a longer transit time in the Triassic aquitard and dissolution of sulfates. On the basis of their chloride, sodium and radon content, Maarouf 1 and 2 represent a mixing zone between the Triassic aquitard and the Liassic aquifer of the Guigo Causse. This mixing zone has a different composition from that of the mixing zone formed at Sbaa in the L'Hajeb Causse, due to a longer transit time.

Khadem seems to be closer to a mixing zone than type I water: the main PCA variables (magnesium, sulfate and nitrate) and the radon content are similar to those of Maarouf while its content in sodium and chloride is lower. The deep well A (Saïs basin), in contact with the Triassic, has an intermediate character between El Mir and, to a lesser extent, Maarouf. This indicates that the groundwater flows mainly take place from the southeast to the northwest but also from the southwest to the northwest.

Interpretation and schematic model of flow paths

Water–rock interactions and mixing zones

A distinction between two spring water types can be made based on chemical analyses and principal component analysis

(Figs. 4 and 9). The first water type arises quasi-exclusively from water–rock interactions within the Liassic limestone-dolomite aquifer and Quaternary travertines. Waters of this group are located in the alignment of Bittit, Ribaa, Aguemguam, Boucharmou and Bou Youssef springs. In contrast, the 2nd water type arises from water–rock interactions with Triassic evaporites. The type II springs are: Maarouf 1 and Maarouf 2, Sbaa, and El Mir. Khadem is distinctive and seems to be intermediate between type I and II waters. Lower Triassic rocks are not exposed in the study area. Water–rock interactions in the Triassic strata take place at a depth that can be obtained from estimates of spring travel time using radon isotopes analyses (Mayer et al. 2014).

The higher ratio (≤ 1.1) of Mg/Ca (Fig. 6) observed in some springs of type I in the western sector is a probable consequence of a more advanced dissolution of dolomite followed by precipitation of calcite, in an aquifer with waters having longer transit times. Another possible mechanism explaining the higher Mg/Ca ratio is the hydrolysis of Mg-rich silicates in Quaternary and Triassic basalts. From the results of principal component analysis (Table 3; Fig. 9) it is shown that magnesium is anti-correlated with silicon; thus, this second mechanism must be eliminated, which is in accordance with a longer transit time in the western sector.

In contrast, the second water type represented by Maarouf, Sbaa, and El Mir (Figs. 4, 5 and 6), shows a net enrichment in Na^+ , K^+ and Cl^- and suggests an interaction with Triassic evaporite formations. Since Triassic rocks do not outcrop in this area, the interaction with Triassic evaporites probably takes place at depth, at the base of the Liassic dolomitic limestone. Groundwater extracted from well A in the Saïs Plain also shows evidence of interactions with Triassic evaporites.

Bicarbonate, nitrate and sulfate concentrations (Table 1; Figs. 4, 5 and 6c) are linked to seasonal variations. All springs have significantly lower concentrations of bicarbonate in March after the rainy season, which is consistent with a higher proportion of groundwater in contact with gypsum and schist near the Triassic aquitard. The increase of nitrate and sulfate after rainy season is particularly true for El Mir spring. Therefore, one can define a Liassic aquifer characterized by waters of type I previously described, and a Triassic aquitard (waters of type II), with two main transition or mixing zones: Sbaa, to the north, and, Maarouf, to the south (Figs. 4 and 5).

^{222}Rn allows us to highlight areas of rapid exchanges between waters flowing into the Liassic aquifer and the Triassic aquitard. The groundwaters in the main mixing areas at extremities (Sbaa, Maarouf) and in the small mixing area of Khadem have higher radon activities (5,500–10,000 Bq/m^3) than if mixing were simply occurring between waters from the Liassic aquifer and the Triassic aquitard. The upwelling time from Triassic aquitard to surface is less than 2 weeks.

Recharge regimes, groundwater reservoir and seasonality

As previously seen, there are recharge areas at five different altitudes. First, the Liassic aquifer contains water (type I) that is regularly renewed from the highest recharge area (1,400 m asl). This recharged water corresponds to Bittit, Ribaa and Aguemguam springs in the L'Hajeb Causse. Isotopic analyses (Fig. 7; Table 2) of these spring sources show they follow the local meteoric water line and suggest a confined aquifer with a rapid and local infiltration (i.e. low evaporation), which explains the observed turbidity problem described after rain events (Amraoui et al. 2003). Secondly, groundwater in contact with the Triassic aquitard (El Mir) presents a recharge zone at lower elevation (1,000 m asl) and a stronger evaporation than the type I waters in the eastern sector. Third, the two

mixing zones at the edges of the basin, corresponding to Sbaa and Maarouf springs, have respectively intermediate recharge altitudes of 1,200 and 900 m asl. Fourth, a fifth recharge zone at 1,040 m asl corresponds to another causee (Guigo Causse) and supplies Boucharmou, Bou Youssef and Khadem; however, isotopic analyses show that these waters are subparallel to the local meteoric line, which indicates high evaporation.

Seasonality is well marked by the change of sulfate (Fig. 6c) and water isotopes ($\delta^{18}\text{O}$, δD ; Fig. 7). The water renewal is still sufficient, as shown by tritium analyses, which characterizes modern waters. However, periods of rain are more intense on shorter time scales (Amraoui et al. 2003; Etebaai et al. 2012), while the droughts are longer; thus, the infiltration in the causes is then less effective. In addition, the development of human activity

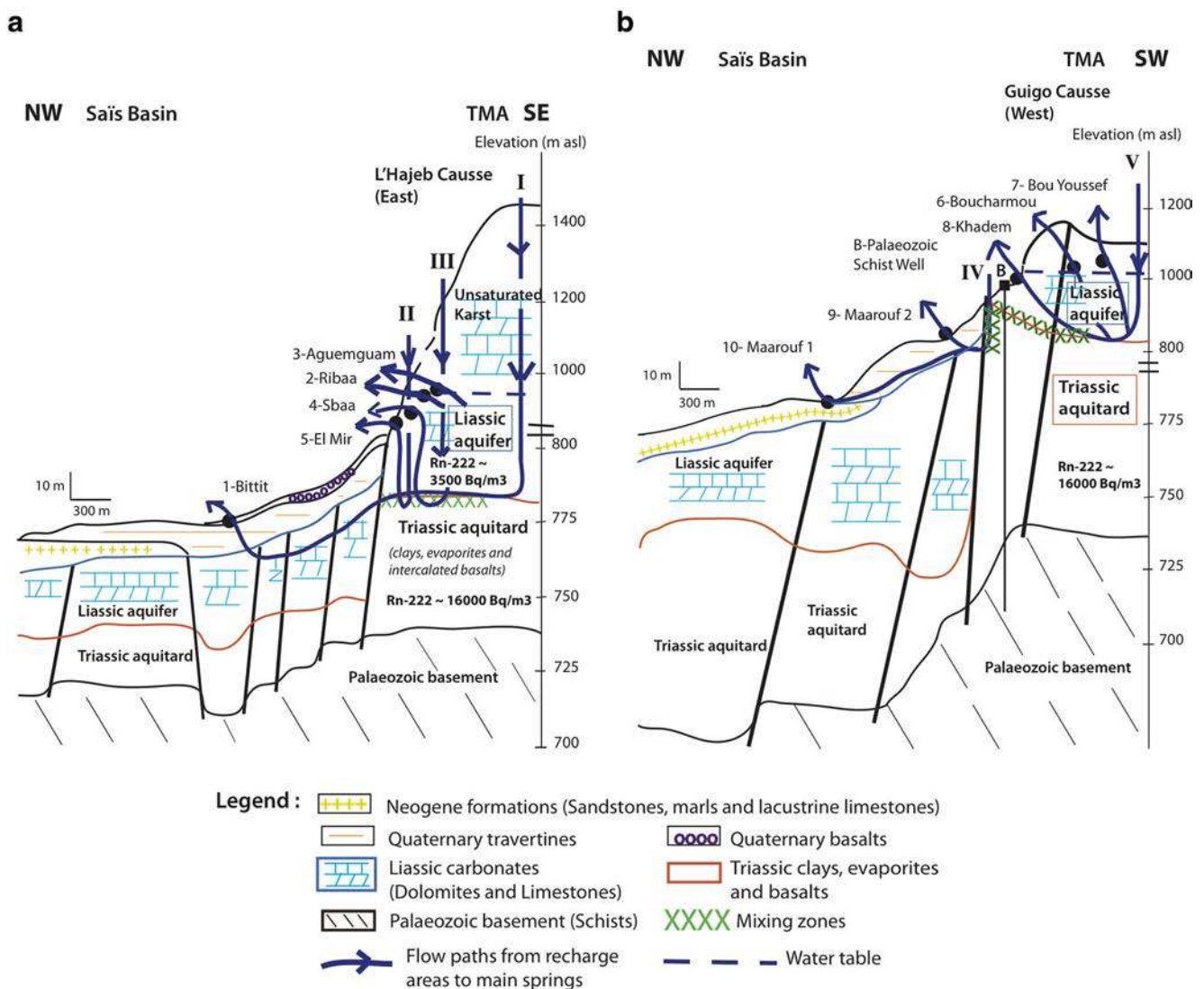


Fig. 10 Conceptual model of groundwater circulation, for **a** L'Hajeb Causse in the east, and for **b** Guigo Causse in the west, with mixing zones between the Middle Atlas Causes and Saïs Basin, from five recharge areas to springs—I to III: L'Hajeb Causse; IV, V: Guigo

Causse. Recharge areas and altitudes: I (1,400 m asl), Bittit, Ribaa, Aguemguam; II (1,000 m asl), El Mir; III (1,200 m asl), Sbaa; IV (900 m asl), Maarouf 1 and 2; V (1,040 m asl), Boucharmou, Bou Youssef, Khadem

plays a major role in the exploitation of groundwater in the Saïb basin and appears to be the dominant factor compared to the climate in the depletion of water resources.

Conceptual model of flow paths

The set of geochemical and isotopic data and the multivariate analyses of data allow for the establishment of a first model (Fig. 10) of groundwater flow for the L'Hajeb Causse (east) and Guigo Causse (west). The model takes into account five highlighted recharge areas, groundwater flow paths to the springs, and the mixing zones.

It is important to note that the causses of this study area were formed in the same period and have a similar geological composition (dolomite, calcite). From a geochemical point of view, dolomite that can hardly reprecipitate (Michalowski and Asuero 2012) shows a difference between the region east and west. Reprecipitation of calcite is favored by longer transit times in the western part of the study area, leading to a higher Mg/Ca ratio in the Liassic aquifer of the Guigo Causse, as confirmed by the geochemical analyses of this study and tritium values from the International Atomic Energy Agency (type I waters).

Radon analyses revealed the existence of rapid exchange areas (less than 12 days) in the mixing zones between the Triassic aquitard and the Liassic aquifer. El Mir spring in L'Hajeb Causse would be typical of the Triassic aquitard of both causses. Indeed, the water of well B in the Triassic aquitard and in contact with the Palaeozoic schists of Guigo Causse, has the same electrical conductivity as type II waters, i.e. the same content in dissolved salt. The Triassic aquitard, probably very discontinuous around El Mir, allows an easy water circulation, as indicated by the radon activities of the mixing zones (Sbaa, Maarouf 1 and 2, and probably Khadem). Because these activities are higher than if it was a simple mixing of waters circulating in Lias and Triassic, one can say that the mixing takes place in the Triassic aquitard.

In L'Hajeb Causse, Sbaa water is in contact with the Liassic confined aquifer and circulates in one mixing zone with the Triassic. In Guigo Causse, which is less high and more rugged, the springs Maarouf 1 and 2 are in contact with the Liassic unconfined aquifer, which is more prone to evaporation, and water probably circulates in multiple mixing zones with the Triassic, as shown by elevated values of electrical conductivity. Khadem spring in Guigo Causse seems to be associated with another mixing zone with a more Liassic character than Maarouf.

The water of both aquifers at the junction between the TMA and the Saïb plain would be in contact between Ribaa and Bou Youssef, probably close to Oued Tizguit, and would circulate slowly from northeast to southwest, and also to a lesser extent from northwest to southwest perpendicular to the causses.

Conclusions and perspective

The geochemical and isotopic study associating a multivariate statistical analysis of the data and a thermodynamic balance of the phases in solution, allowed for characterization of the studied system of 10 springs and 3 wells (over an area 70×40 km) at the junction of Saïb Basin and the Middle Atlas Causses. The study showed the existence of several aquifers of Liassic origin and a few reservoirs in the Triassic aquitard, and pointed toward two different karstic hydrological systems associated with L'Hajeb and Guigo Causses. Two main mixing zones at the edges of the system are highlighted: Sbaa to the east, and Maarouf 1 and 2 to the west. Khadem to the west seems to be also a small mixing zone.

The study highlighted the existence of areas of rapid exchange between waters of Liassic aquifers and waters in contact with the Triassic aquitard. The upwelling time from the Triassic aquifer is less than 12 days (from ^{222}Rn data). These results are consistent with the time scale of seasonal rainfall events observed in the geochemistry of spring waters and explain turbidity problems (Amraoui et al. 2003) after strong rain episodes.

Deuterium excess characterizes a local recharge of the groundwater. Waters in the Liassic aquifer have a lighter isotopic composition than waters in contact with Triassic evaporites. This difference characterizes a higher altitude of recharge for karstic waters. Five altitudes of recharge have been identified; moreover, it is inferred that there is a drain (or preferential flow) of waters perpendicular to the causses in the Bittit-Ribaa area (Qarqori et al. 2012; Qarqori 2015).

The influence of climate is difficult to assess given the lack of data on previous years for the whole basin and causses. Groundwater is primarily recharged by large rainfall events; nevertheless, the impact of human activity plays a more active role than the one of seasonal variations in the Ribaa-Bittit complex.

Finally, a first conceptual model of the flow paths from recharge areas to springs in this karst system is presented. To improve the model and to obtain a better understanding of groundwater recharge and flow, installation of monitoring instruments at wells and springs, with recording of stage, temperature, and rainfall at regular intervals (at least daily), is necessary.

Acknowledgements We want to particularly thank Yves Travi (EMMAH-Avignon University PAV, France) for his advice in our isotopic analyses, Mustapha Boujamaoui (FST-Errachidia, University MI, Maroc) for his efficient help during our measurement acquisitions, and Clément Layet and Ghislain Gassier (CEREGE) for fruitful discussions on the PCA method. We also acknowledge the reviewers for their useful remarks. This work was developed in the Program of "Fédération de Recherche" ECCOREV No. 3058 of CNRS -Centre National de la Recherche Scientifique-France, and BREMEX project of the "Conseil Régional PACA, France".

References

- Agence du Bassin Hydraulique du Sebou-Fes (2008–2011) Situation Hydrologique du Bassin du Sebou, années hydrologiques 2008/2009, 2009/2010, 2010/2011. [Hydrological situation of the Sebou Basin, hydrological years 2008/2009, 2009/2010, 2010/2011]. Agence du Bassin Hydraulique du Sebou-Fes, Rabat, Morocco
- Amraoui F (2005) Contribution à la connaissance des aquifères karstiques: cas du Lias de la plaine du Saïs et du Causse Moyen Atlasique tabulaire (Maroc) [Contribution to the knowledge of karstic aquifers: case of the Lias of the Saïs plain and the middle atlas Moyen Causse (Morocco)]. PhD Thesis, Université Hassan II Ain Chock, Casablanca, Morocco
- Amraoui F, Razack M, Bouchaou L (2005) Impact of a long drought period on a large carbonate aquifer: the Liassic aquifer of the Saïs plain and middle atlas plateau (Morocco). In: Regional hydrological impacts of climatic change: hydroclimatic variability, IAHS Publ. 296, IAHS, Wallingford, UK, pp 184–193
- Amraoui F, Razack M, Bouchaou L (2004) Behaviour of a karstic spring subjected to a long drought period: Bittit spring (Morocco). *C R Geosci* 336:1099–1109
- Amraoui F, Razack M, Bouchaou L (2003) Turbidity dynamics in karstic systems: example of Ribaa and Bittit springs in the middle atlas (Morocco). *Hydrological Sci J* 48(6):971–984
- Bahaj T, Wartiti M, Zahraoui M, Essahlaoui A, Caboi R (2004) Aspects of groundwater geochemistry from Middle Atlas and Saiss basin (Northern Morocco). In: RB Wanty, RR Seal II (eds) Water–rock interaction. Taylor and Francis, London, pp 343–346
- Belkhir A (2007) Gestion intégrée des ressources en eau, protection de la ressource: bassin du Sebou [Integrated water resources management, resource protection: Sebou Basin]. *Rev HTE* 137:9–22
- Benaabidate L, Fryar AE (2010) Controls on ground water chemistry in the central couloir Sud Rifain, Morocco. *Ground Water* 48(2):306–319
- Bentayeb A, Leclerc C (1977) Le Causse moyen-atlasique [The Middle-Atlas Causse]. In: Ressources en Eau du Maroc, Domaines atlasique et sud-atlasique, tome 3 [Morocco Water Resources, Atlas and South Atlas areas, vol 3]. Moroccan Geological Survey Publ. 231, pp 37–84
- Bzioui M (2004) Rapport national sur les ressources en eau au Maroc [National report about Morocco's water resources]. UN Water, Geneva, 94 pp
- Chamayou J, Combe M, Jenetier B, Leclerc C (1975) Le bassin de Meknes-Fès [The Meknes-Fes basin]. In: Ressources en eau du Maroc, Plaines et bassins du Maroc atlantique, tome 2. Notes et Mémoires du Service Géologique, n° 231 [Morocco water resources, plains and basins of Atlantic Morocco, vol 2. Notes and Memoirs of the Geological Survey, no. 231]. Moroccan Geological Survey, Rabat, pp 41–71
- Craig H, Gordon LI (1965) Deuterium and oxygen-18 variations in the ocean and the marine atmosphere. In: Stable isotopes in oceanography studies and paleotemperatures: Spoleto 1965. 26–30 July 1965, Spoleto, Italy, pp 9–130
- Damnati B, Etebaai I, Reddad H, Benhardouz H, Benhardouz O, Miche H, Taieb M (2012) Recent environmental changes and human impact since mid-20th century in Mediterranean lakes: Ifrah, Iffer and Afourgagh, Middle Atlas Morocco. *Quat Int* 262:44–55. <https://doi.org/10.1016/j.quaint.2011.09.028>
- Dansgaard W (1964) Stable isotopes in precipitation. *Tellus XVI* 4:436–468
- Dauteuil O, Moreau F, Qarqori K (2016) Structural pattern of the Saiss basin and Tabular Middle Atlas in northern Morocco: hydrological implications. *J Afr Earth Sci* 119:150–159
- De Jong C, Cappy S, Finckh M, Funk D (2008) A transdisciplinary analysis of water problems in the mountainous karst areas of Morocco. *Eng Geol* 99:228–238. <https://doi.org/10.1016/j.enggeo.2007.11.021>
- Drogue C (1969) Contribution à la connaissance hydrogéologique de quelques karsts du midi-méditerranéen Français [Contribution to the hydrogeological knowledge of some karsts in the French Mediterranean]. PhD Thesis, Université de Montpellier, Montpellier, France
- El Ouali A, Sefrioui S, Mudry J, Fassi Fihri O, Essahlaoui A, Marah H (2014) Contribution of isotopes of the water molecule to determine recharge altitude of the Main Springs welling up in the Middle Atlas limestone (Morocco). In: Mudry J, Zwahlen F, Bertrand C, LaMoreaux J (eds) H2Karst Research in Limestone Hydrogeology. Environmental Earth Sciences, Springer, Cham, Switzerland, pp 59–68
- Esper J, Franck D, Buntgen U, Verstege A, Luterbacher J, Xoplaki E (2007) Long-term drought severity variations in Morocco. *Geophys Res Lett* 14:L17702. <https://doi.org/10.1029/2007GL030844>
- Essahlaoui A, Sahbi H, Bahi L, El-Yamine N (2001) Preliminary survey of the structure and hydrogeology of the western Saïs basin, Morocco, using electrical resistivity. *J Afr Earth Sci* 32(4):777–789
- Etebaai I, Damnati B, Raddad H, Benhardouz H, Benhardouz O, Miche H, Taieb M (2012) Climatic and human impacts on the hydrogeochemical functioning of Lake Ifrah (Middle Atlas, Morocco). *Hydrol Sci J* 57(3):547–561. <https://doi.org/10.1080/02626667.2012.660158>
- Georgin JP (2007) Analyse interactive des données (ACP, AFC) avec Excel 2000, Théorie et pratique [Data interactive analysis (PCA, CFA) with Excel 2000, theory and practice], 2nd edn. Presses Universitaires de Rennes, Rennes, France
- Hoehn E, Von Gunten HR (1989) Radon in groundwater: a tool to assess infiltration from surface waters to aquifers. *Water Resour Res* 25(8): 1795–1803
- Hubert P, Olive P (1995) Modélisation par une loi gamma de la distribution des temps de séjour de l'eau dans des systèmes hydrogéologiques en régime permanent [Modeling by a gamma law of the distribution of water transit times in steady-state hydrogeological systems]. Tracer Technologies for Hydrological Systems. IAHS Publ. 229, IAHS, Wallingford, UK, pp 211–217
- IAEA (2010) Atlas of isotope hydrology, Morocco, Sebou basin. IAEA, Vienna, pp 19–124
- Kabbaj A, Combe M (1977) Le domaine atlasique: présentation du domaine atlasique [The Atlas area: introduction to the Atlas area]. In: Ressources en eau du Maroc, domaines atlasique et sud-atlasique, tome 3. Notes et Mémoires du Service Géologique du Maroc, n° 231 [Morocco Water resources, Atlas and South Atlas areas, vol 3. Notes and Memoirs of the Moroccan Geological Survey, no. 231]. Moroccan Geological Survey, Rabat, Morocco, pp 29–36
- Lucas LL, Unterweger MP (2000) Comprehensive review and critical evaluation of the half-life of tritium. *J Res Natl Inst Stand Technol* 105(4):541–549. <https://doi.org/10.6028/jres.105.043>
- Luterbacher J, et al. (2006) Mediterranean climate variability over the last centuries: a review. In: Lionello P, Malanotte-Rizzoli P, Boscolo R (eds) The Mediterranean climate: an overview of the main characteristics and issues. Elsevier, Amsterdam, pp 27–148
- Martin J (1981) Le Moyen Atlas Central, Etude géomorphologique, Notes et Mémoires du Service Géologique du Maroc, Rabat [The Central Middle Atlas, Geomorphological study]. Notes and Memoirs of the Geological Survey, no. 258, Moroccan Geological Survey, Rabat, Morocco, pp 17–265
- Mayer A, Sültenfuß J, Travi Y, Rebeix R, Purtschert R, Claude C, Le Gal La Salle C, Miche H, Conchetto E (2014) A multi-tracer study of groundwater origin and transit-time in the aquifers of the Venice

- region (Italy). *Appl Geochem J* 50:177–198. <https://doi.org/10.1016/j.apgeochem.2013.10.009>
- Michalowski T, Asuero AG (2012) Thermodynamic modelling of dolomite behavior in aqueous media. *J Thermodynam* 2012:723052, 12 pp. <https://doi.org/10.1155/2012/723052>
- Parkhurst DL, Appelo CAJ (1999) User's guide to PHREEQC (version 2): a computer program for speciation, batch-reaction, one-dimensional transport, and inverse geochemical calculations. US Geol Surv Water Resour Invest Rep 99-4259
- Qarqori Kh, Rouai M, Moreau F, Saracco G, Dauteuil O, Hermitte D, Boualoul M, Le Carlier de Veslud C (2012) Geoelectrical tomography investigating and modeling of fractures network around Bittit spring (Middle Atlas, Morocco). *Int J Geophys* 489634, 13 pp. <https://doi.org/10.1155/2012/489634>
- Qarqori KH (2015) Contribution à l'étude du réservoir discontinu et karstique des causses Moyen-Atlasiques et de sa jonction avec le bassin de Saïs par télédétection spatiale et imagerie géophysique [Contribution to the study of the discontinuous and karstic reservoir of the Middle Atlasic Causses and its junction with the Saïs basin by remote sensing and geophysical imagery]. PhD Thesis, Université Moulay Ismail, Meknès, Morocco
- Rosenberg YO, Metz V, Ganor J (2013) Radium removal in a large scale evaporitic system. *Geochim Cosmochim Acta* 103:121–137. <https://doi.org/10.1016/j.gca.2012.10.046>
- Rozanski, K, Araguás-Araguás L, Gonfiantini R (1993) Isotopic patterns in modern global precipitation. In: Swart PK, et al. (eds) *Climate change in continental isotopic records*. Geophys. Monogr. Ser., vol 78, AGU, Washington, DC, pp 1–36
- Savoy L, Surbeck H, Hunkeler D (2011) Radon and CO₂ as natural tracers to investigate the recharge dynamics of karst aquifers. *J Hydrol* 406:148–157. <https://doi.org/10.1016/j.jhydrol.2011.05.031>
- Sefrioui S, Fassi Fihri O, El Ouali A, Marah H, Newman B, Essahlaoui A (2010) Utilisation des outils isotopiques pour la détermination de l'altitude de recharge des principales sources du bassin de Sebou-Moroc [Use of isotopic tools to determine the altitude of recharge of the main springs in the Sebou-Morocco basin]. *Revue Geomaghreb* 6:79–96
- Simler R (2012) Software "Diagrammes" V. 5.9. LHA, EMMAH, UAPV Avignon, France
- Tadolini T, Spizzico M (1998) Relation between "terra rossa" from the Apulia aquifer of Italy and the radon content of groundwater: experimental results and their applicability to radon occurrence in the aquifer. *Hydrogeol J* 6(3):450–454

Hydrochemical constraints between the karst Tabular Middle Atlas Causses and the Saïs basin (Morocco): implications of groundwater circulation

Hélène Miche ¹✉, Ginette Saracco ¹, Adriano Mayer ^{1,2}, Khaoula Qarqori ³, Mohamed Rouai ³,
Abdelilah Dekayir ³, Konstantinos Chalikakis ², Christophe Emblanch ²

¹ CNRS-UMR 7330, CEREGE, Aix-Marseille Université, IRD, Europôle de l'Arbois, BP 80,
13545 Aix en Provence cedex 4, France, miche@cerege.fr, saracco@cerege.fr

² Université d'Avignon et des Pays de Vaucluse, INRA, EMMAH, UMR 1114, LHA, 84000
Avignon, France adriano.mayer@univ-avignon.fr, konstantinos.chalikakis@univ-avignon.fr,
christophe.emblanch@univ-avignon.fr

³ Université Moulay Ismail, Faculté des Sciences, Département des Sciences de la Terre, BP
11201, 50000 Meknès, Maroc, khqarqori@gmail.com, mohamed.rouai@laposte.net,
dekayir@yahoo.fr

Hélène Miche✉ : contact author, miche@cerege.fr

Table S1 Saturation indexes determined with PHREEQC version 2.7 (database Wateq.dat), for phases in springs and wells of the sampling campaigns (2009-2010). Samples of springs and wells are referenced with the same codes as in Table 1 of the main article. Phases of interest in bold characters: aragonite, calcite, dolomite, quartz and cristobalite

Table S1

Saturation indexes Samples	Bittit spring			Ribaa spring		Aguemguam spring			Sbaa spring		El Mir spring		
	1.1	1.2	1.3	2.1	2.2	3.1	3.2	3.3	4.1	4.2	5.1	5.2	5.3
Anhydrite	-3.36	-3.22	-3.28	-3.34	-3.18	-3.36	-3.22	-3.39	-3.10	-2.96	-3.38	-2.93	-3.03
Aragonite	-0.12	-0.09	0.02	0.26	0.34	-0.11	-0.18	0.05	-0.11	-0.26	-0.28	-0.27	-0.05
Artinite	-7.46	-6.97	-6.69	-6.08	-5.58	-7.39	-7.35	-6.62	-7.34	-7.52	-7.69	-7.59	-6.88
Barite	-2.41	*	-2.24	-2.38	*	-2.48	*	-2.34	-2.22	*	-2.52	*	-1.98
Brucite	-6.12	-5.63	-5.50	-5.14	-4.71	-6.06	-5.91	-5.46	-6.00	-6.03	-6.16	-6.06	-5.58
Calcite	0.03	0.07	0.17	0.41	0.49	0.04	-0.03	0.20	0.04	-0.11	-0.13	-0.13	0.10
Celestite	-4.62	*	-4.47	-4.60		-4.63	*	-4.59	-4.48	*	-4.35	*	-3.96
Chalcedony	-0.49	-0.43	-0.43	-0.46	-0.39	-0.47	-0.32	-0.44	-0.64	-0.75	-0.40	-0.39	-0.40
Chrysotile	-7.68	-6.09	-5.68	-4.68	-3.27	-7.45	-6.66	-5.54	-7.74	-8.06	-7.72	-7.39	-5.96
Clinoenstatite	-4.62	-4.07	-3.93	-3.61	-3.11	-4.54	-4.23	-3.90	-4.66	-4.80	-4.57	-4.46	-3.99
CO ₂ (g)	-1.64	-2.15	-2.14	-2.24	-2.58	-1.72	-2.01	-2.18	-1.64	-1.75	-1.67	-1.79	-2.05
Cristobalite	-0.44	-0.38	-0.38	-0.41	-0.34	-0.42	-0.26	-0.38	-0.59	-0.70	-0.35	-0.34	-0.35
Diopside	-6.15	-5.01	-4.79	-4.14	-3.15	-5.99	-5.31	-4.70	-6.27	-6.56	-6.07	-5.85	-4.90
Dolomite	-0.06	-0.03	0.22	0.72	0.87	-0.04	-0.23	0.29	-0.01	-0.32	-0.38	-0.37	0.08
Dolomite(d)	-0.64	-0.61	-0.37	0.13	0.29	-0.63	-0.82	-0.30	-0.59	-0.89	-0.95	-0.95	-0.50
Epsomite	-5.63	-5.53	-5.54	-5.60	-5.44	-5.62	-5.53	-5.64	-5.40	-5.26	-5.70	-5.25	-5.35
Forsterite	-10.89	-9.86	-9.59	-8.90	-7.98	-10.76	-10.30	-9.52	-10.81	-10.98	-10.87	-10.67	-9.72
Gypsum	-3.12	-2.97	-3.04	-3.10	-2.93	-3.11	-2.97	-3.14	-2.86	-2.72	-3.14	-2.69	-2.79
H ₂ (g)	-22.36	-22.90	-23.00	-23.34	-23.76	-22.44	-22.66	-23.08	-22.30	-22.26	-22.18	-22.32	-22.80
H ₂ O(g)	-1.73	-1.74	-1.74	-1.73	-1.73	-1.74	-1.75	-1.76	-1.68	-1.67	-1.67	-1.68	-1.68
Halite	-8.78	-8.84	-8.82	-8.77	-9.08	-8.82	-8.91	-8.96	-8.34	-8.43	-6.24	-6.38	-6.14
Huntite	-4.60	-4.58	-4.04	-3.05	-2.73	-4.58	-5.01	-3.93	-4.48	-5.08	-5.23	-5.23	-4.33
Hydromagnesite	-15.20	-14.74	-14.02	-12.66	-11.92	-15.12	-15.45	-13.87	-14.99	-15.61	-15.91	-15.82	-14.43
Magadiite	-11.10	-10.48	-10.47	-10.43	-9.87	-11.02	-9.90	-10.53	-11.82	-12.67	-9.10	-9.05	-8.80
Magnesite	-0.64	-0.64	-0.50	-0.25	-0.17	-0.63	-0.75	-0.47	-0.62	-0.76	-0.81	-0.81	-0.58
Mirabilite	-10.45	-10.38	-10.49	-10.44	-10.60	-10.51	-10.44	-10.59	-9.94	-9.99	-8.08	-7.72	-7.62
Nahcolite	-5.21	-5.48	-5.45	-5.32	-5.61	-5.28	-5.49	-5.46	-5.07	-5.29	-4.10	-4.20	-4.12
Natron	-11.03	-11.06	-11.01	-10.65	-10.90	-11.09	-11.22	-10.98	-10.75	-11.10	-8.79	-8.88	-8.46
Nesquehonite	-3.04	-3.04	-2.90	-2.65	-2.57	-3.03	-3.15	-2.87	-3.02	-3.17	-3.21	-3.21	-2.98
O ₂ (g)	-41.33	-40.35	-40.19	-39.44	-38.49	-41.35	-41.05	-40.25	-40.77	-40.78	-40.90	-40.80	-39.88
Portlandite	-12.04	-11.51	-11.42	-11.06	-10.63	-11.98	-11.79	-11.39	-11.88	-11.92	-12.01	-11.92	-11.44
Quartz	-0.03	0.02	0.02	-0.00	0.06	-0.02	0.14	0.02	-0.19	-0.30	0.05	0.06	0.05
Sepiolite	-5.84	-4.67	-4.39	-3.78	-2.73	-5.63	-4.83	-4.28	-6.20	-6.60	-5.80	-5.54	-4.60
Sepiolite(d)	-8.52	-7.34	-7.06	-6.45	-5.41	-8.30	-7.49	-6.93	-8.93	-9.33	-8.54	-8.27	-7.32
Silicagel	-1.03	-0.97	-0.97	-1.00	-0.93	-1.01	-0.86	-0.98	-1.18	-1.29	-0.94	-0.93	-0.94
SiO ₂ (a)	-1.36	-1.30	-1.30	-1.33	-1.26	-1.34	-1.19	-1.31	-1.50	-1.61	-1.26	-1.25	-1.26
Strontianite	-2.68	*	-2.47	-2.29	*	-2.68	*	-2.45	-2.79	*	-2.56	*	-2.29
Talc	-5.08	-3.37	-2.96	-2.01	-0.46	-4.81	-3.72	-2.84	-5.41	-5.93	-4.90	-4.56	-3.15
Thenardite	-11.79	-11.73	-11.85	-11.79	-11.93	-11.88	-11.82	-11.98	-11.18	-11.23	-9.31	-8.98	-8.88
Thermonatrite	-12.85	-12.90	-12.85	-12.48	-12.72	-12.93	-13.09	-12.85	-12.48	-12.82	-10.51	-10.62	-10.20
Tremolite	-12.48	-8.47	-7.62	-5.37	-1.85	-11.87	-9.41	-7.30	-13.10	-14.22	-12.22	-11.41	-8.10
Trona	-18.08	-18.41	-18.34	-17.84	-18.34	-18.26	-18.64	-18.37	-17.47	-18.03	-14.52	-14.76	-14.26

Table S1 (continued)

Saturation indexes	Boucharmou spring		Bou Youssef spring		Maarouf 1 spring		Maarouf 2 spring		Khadem spring	HajKaddour (deep w.)	Palaeozoic schist w.		Basaltic schist w.
	6.1	6.2	7.1	7.2	9.1	9.2	10.1	10.2	8	A	B.1	B.2	C
Anhydrite	-2.98	-2.49	-2.87	-2.83	-2.79	-2.74	-3.01	-2.89	-3.53	-2.88	-1.72	-1.52	-2.86
Aragonite	0.05	0.32	-0.02	-0.04	-0.17	-0.22	-0.13	-0.19	-0.99	-0.07	0.29	-0.34	0.19
Artinite	-6.36	-5.11	-6.72	-6.46	-6.81	-6.65	-6.77	-6.52	-6.53	-6.36	-5.71	-7.80	-7.25
Barite	-2.14	*	-1.96	*	-1.69	*	-0.88	*	*	-1.73	-0.17	-0.40	-1.73
Brucite	-5.36	-4.36	-5.56	-5.27	-5.61	-5.39	-5.62	-5.31	-5.32	-5.19	-4.64	-5.88	-5.73
Calcite	0.20	0.47	0.13	0.11	-0.02	-0.08	0.01	-0.04	-0.84	0.07	0.44	-0.20	0.34
Celestite	-4.14	*	-4.22	*	-3.88	*	-5.13	*	*	-3.73	-2.05	-2.25	-4.24
Chalcedony	-0.78	-0.79	-0.82	-0.76	-0.67	-0.73	-0.68	-0.71	-0.79	-0.66	-0.34	-0.40	-0.35
Chrysotile	-6.09	-3.10	-6.72	-5.70	-6.69	-6.14	-6.74	-5.88	-5.94	-5.75	-3.13	-7.22	-6.31
Clinoenstatite	-4.15	-3.17	-4.39	-4.04	-4.30	-4.14	-4.33	-4.05	-4.13	-3.91	-3.01	-4.33	-4.10
CO ₂ (g)	-1.93	-2.71	-1.97	-2.32	-1.82	-2.09	-1.76	-2.12	-2.26	-1.83	-2.66	-1.97	-2.14
Cristobalite	-0.73	-0.74	-0.77	-0.71	-0.62	-0.68	-0.64	-0.66	-0.74	-0.63	-0.30	-0.36	-0.31
Diopside	-5.44	-3.43	-5.80	-5.07	-5.77	-5.45	-5.84	-5.28	-6.19	-5.06	-2.86	-5.39	-4.64
Dolomite	0.49	1.00	0.23	0.18	0.08	-0.03	0.16	0.05	-0.79	0.29	0.67	-0.75	0.09
Dolomite(d)	-0.09	0.42	-0.35	-0.40	-0.49	-0.60	-0.41	-0.52	-1.37	-0.26	0.10	-1.30	-0.49
Epsomite	-5.10	-4.64	-5.08	-5.05	-4.91	-4.85	-5.11	-5.00	-4.81	-5.13	-4.16	-4.22	-5.64
Forsterite	-9.66	-7.67	-10.11	-9.46	-10.06	-9.67	-10.09	-9.50	-9.60	-9.21	-7.80	-10.33	-9.97
Gypsum	-2.74	-2.25	-2.63	-2.59	-2.56	-2.50	-2.77	-2.66	-3.29	-2.67	-1.48	-1.30	-2.62
H ₂ (g)	-22.92	-23.94	-22.82	-23.16	-22.54	-22.76	-22.54	-22.84	-23.04	-22.62	-23.62	-22.00	-23.04
H ₂ O(g)	-1.67	-1.68	-1.70	-1.71	-1.64	-1.64	-1.64	-1.64	-1.70	-1.47	-1.64	-1.51	-1.69
Halite	-9.25	-9.00	-9.24	-9.18	-7.63	-7.58	-7.26	-7.22	-8.93	-6.53	-6.65	-6.73	-8.76
Huntite	-3.31	-2.31	-3.93	-4.06	-4.08	-4.31	-3.90	-4.13	-5.04	-3.62	-3.24	-6.20	-4.79
Hydromagnesite	-12.99	-11.02	-13.90	-13.76	-14.00	-14.01	-13.81	-13.74	-13.85	-13.18	-12.51	-16.93	-15.50
Magadiite	-12.94	-12.51	-13.40	-12.78	-11.43	-11.71	-11.35	-11.35	-12.94	-10.23	-8.19	-9.16	-9.73
Magnesite	-0.28	-0.03	-0.45	-0.49	-0.47	-0.52	-0.42	-0.48	-0.50	-0.37	-0.34	-1.13	-0.81
Mirabilite	-10.66	-10.10	-10.58	-10.38	-8.88	-8.80	-8.68	-8.56	-9.99	-8.07	-7.13	-7.84	-10.24
Nahcolite	-5.56	-5.77	-5.63	-5.73	-4.80	-4.96	-4.55	-4.76	-5.64	-4.28	-4.66	-5.06	-5.44
Natron	-11.44	-11.09	-11.55	-11.40	-10.06	-10.10	-9.61	-9.66	-11.27	-9.03	-8.93	-10.44	-11.00
Nesquehonite	-2.68	-2.44	-2.86	-2.89	-2.87	-2.93	-2.82	-2.88	-2.90	-2.78	-2.74	-3.54	-3.21
O ₂ (g)	-39.39	-37.49	-40.08	-39.51	-39.80	-39.36	-39.80	-39.16	-39.64	-37.41	-37.67	-39.19	-39.43
Portlandite	-11.41	-10.39	-11.54	-11.23	-11.67	-11.45	-11.69	-11.39	-12.22	-11.12	-10.38	-11.35	-11.12
Quartz	-0.33	-0.34	-0.37	-0.31	-0.22	-0.28	-0.24	-0.26	-0.34	-0.24	0.10	0.03	0.10
Sepiolite	-5.35	-3.36	-5.78	-4.99	-5.60	-5.33	-5.66	-5.13	-5.22	-5.21	-2.69	-5.69	-4.76
Sepiolite(d)	-8.09	-6.09	-8.48	-7.69	-8.37	-8.10	-8.43	-7.90	-7.92	-8.15	-5.45	-8.59	-7.48
Silicagel	-1.32	-1.33	-1.36	-1.30	-1.20	-1.26	-1.22	-1.25	-1.33	-1.20	-0.88	-0.93	-0.89
SiO ₂ (a)	-1.64	-1.65	-1.68	-1.63	-1.52	-1.58	-1.54	-1.56	-1.66	-1.50	-1.20	-1.24	-1.22
Strontianite	-2.42	*	-2.67	*	-2.57	*	-3.58	*	*	-2.26	-1.36	-2.41	-2.50
Talc	-4.03	-1.07	-4.76	-3.63	-4.39	-3.96	-4.48	-3.66	-3.93	-3.36	-0.19	-4.32	-3.41
Thenardite	-11.88	-11.34	-11.88	-11.69	-10.06	-9.98	-9.85	-9.73	-11.28	-8.93	-8.31	-8.77	-11.50
Thermonatrite	-13.15	-12.82	-13.33	-13.19	-11.72	-11.76	-11.27	-11.32	-13.04	-10.39	-10.59	-11.87	-12.75
Tremolite	-10.08	-3.09	-11.48	-8.87	-11.15	-10.08	-11.37	-9.43	-11.43	-8.91	-1.12	-10.48	-7.84
Trona	-18.62	-18.52	-18.93	-18.92	-16.39	-16.58	-15.68	-15.93	-18.66	-14.22	-15.12	-16.56	-18.14